Thompson Sampling with Diffusion Generative Prior

Yu-Guan Hsieh *
Université Grenoble Alpes
yu-guan.hsieh@univ-grenoble-alpes.fr

Shiva Prasad Kasiviswanathan
Amazon
kasivisw@gmail.com

Branislav Kveton
AWS AI Labs
bkveton@amazon.com

Patrick Blöbaum
Amazon
bloebp@amazon.com

Abstract

In this work, we initiate the idea of using denoising diffusion models to learn priors for online decision making problems. Our special focus is on the meta-learning for bandit framework, with the goal of learning a strategy that performs well across bandit tasks of a same class. To this end, we train a diffusion model that learns the underlying task distribution and combine Thompson sampling with the learned prior to deal with new tasks at test time. Our posterior sampling algorithm is designed to carefully balance between the learned prior and the noisy observations that come from the learner's interaction with the environment. To capture realistic bandit scenarios, we also propose a novel diffusion model training procedure that trains even from incomplete and/or noisy data, which could be of independent interest. Finally, our extensive experimental evaluations clearly demonstrate the potential of the proposed approach.

*Work done during internship at Amazon.

Contents

1 Introduction

Uncertainty quantification is an integral part of online decision making and forms the basis of various online algorithms that trade-off exploration against exploitation. Among these methods, Bayesian approaches allow us to quantify the uncertainty using probability distributions, with the help of the powerful tools of Bayesian inference. Nonetheless, their performance is known to be sensitive to the choice of prior.

For concreteness, let us consider the problem of stochastic multi-armed bandits (MABs) [Bubeck and Cesa-Bianchi, 2012, Lattimore and Szepesvári, 2020], in which a learner repeatedly pulls one of the K arms from a given set $\mathcal{A} = \{1, ..., K\}$ and receives rewards that depend on the learner's choices. More precisely, when arm a is pulled at round t, the learner receives reward $r_t \in \mathbb{R}$ drawn from an arm-dependent distribution $\mathcal{P}^a$. The goal of the learner is either to *i*) accumulate the highest possible reward over time (a.k.a. regret-minimization) or to *ii*) find the arm with the highest expected reward within a prescribed number of rounds (a.k.a. best-arm identification).

For both purposes, we need to have a reasonable estimate of the arms' mean rewards $\mu^a = \mathbb{E}_{r^a \sim \mathcal{P}^a}[r^a]$. In general, this would require us to pull each arm a certain number of times, which becomes inefficient when K is large. While the no-free-lunch principle prevents us from improving upon this bottleneck in general situations, it is worth noticing that the bandit instances (referred as tasks hereinafter) that we encounter in most practical problems are far from arbitrary. To name a few examples, in recommendation systems, each task corresponds to a user with certain underlying preferences that affect how much they like each item; in online shortest path routing, we operate in real-world networks that feature specific characteristics. In this regard, introducing such *inductive bias* to the learning algorithm would be beneficial. In Bayesian models, this can be expressed through the choice of the prior distribution. Moreover, as suggested by the mete-learning paradigm, the prior itself can also be learned from data, which often leads to superior performance [Rothfuss et al., 2021, Hospedales et al., 2021]. This has led to the idea of meta-learning a prior for bandits [Peleg et al., 2022, Cella et al., 2020, Basu et al., 2021].

On the other hand, we have recently witnessed the success of deep generative modeling in producing high-quality synthetic data across various modalities [Saharia et al., 2022, Wu et al., 2021, Brown et al., 2020]. The impressive results shows that these models come out as a powerful tool for modeling complex distributions. While different models have their own strength and weakness, diffusion models [Sohl-Dickstein et al., 2015, Ho et al., 2020] turn out to be particularly appealing for our use case as its iterative sampling scheme makes it much more flexible to be applied on a downstream task. In this regard, this paper attempts to answer the following question:

Can diffusion models provide better priors to address the exploration-exploitation trade-off in bandits?

Our Contributions. In this work, we initiate the idea of using diffusion models to meta-learn a prior for bandit problems. Working towards this direction, we make the following contributions:

- We propose a new Thompson sampling scheme that incorporates a prior represented by a diffusion model. The designed algorithm strikes a delicate balance between the learned prior and bandit observations, bearing in mind the importance of having an accurate uncertainty estimate. In particular, the deployment of the diffusion model begins with a variance calibration step. Then, in each round of the interaction we summarize the interaction history by a masked vector of dimension K, and perform posterior sampling with a modified iterative sampling process that makes use of this vector in each step.
- Standard diffusion model training assumes access to noise-free samples. This is however nearly impossible in most bandit applications. To overcome this limitation, we propose a novel diffusion model training procedure which only utilizes incomplete and/or noisy observations. Our method alternates between sampling from the posterior distribution and minimizing a modified loss function that is suited to imperfect data. We believe that this training procedure could be of interest beyond bandit setup for example in deep generative modeling scenarios where noise-free training data are not accessible or expensive to get.

- We perform extensive experimental evaluations on various synthetic and real datasets to demonstrate the benefit of the considered approach against several baseline methods including Thomspon sampling with Gaussian priors [Thompson, 1933], Thompson sampling with Gaussian mixture model (GMM) priors [Hong et al., 2022b], and UCB [Auer, 2002]. The results confirm that the use of diffusion prior always leads to improved performance and the improvement is particularly significant when the underlying problem has a complex structure.

Related Work. Prior to our work, the use of diffusion models in decision making has been explored by Janner et al. [2022], Ajay et al. [2022], who used conditional diffusion models to synthesize trajectories in offline decision making. Their approaches demonstrated good performance on various benchmarks. In contrast, our focus is on online decision making, where exploration is crucial for the success of the algorithm. Additionally, we use diffusion models to learn a task prior, rather than a distribution specific to a single task.

More generally, diffusion models have been used as priors in various areas, primarily for the goal of inverse problem solving. Our posterior sampling algorithm shares some similarity with those presented in previous studies by Sohl-Dickstein et al. [2015], Song et al. [2021], Chung et al. [2022a]. Essentially, these algorithms combine each unconditional sampling step with a step that ensures coherence with the observation. Alternatively, close form expression for the conditional score function and the conditional reverse step can be derived if we assume the observed noise is carved from the noise of the diffusion process. This approach was taken by Kawar et al. [2021, 2022]. Another solution is to approximate the posterior with a Gaussian distribution, as proposed by Graikos et al. [2022]. In this case, samples are reconstructed by minimizing a weighted sum of the denoising loss and a constraint loss, rather than using an iterative sampling scheme.

Regarding the algorithmic framework, we build upon the well-known Thompson sampling idea introduced by Thompson [1933] nearly a century ago. It has reemerged as one of the most popular algorithms for bandit problems in the last decade due to its simplicity and generality [Chapelle and Li, 2012, Russo and Van Roy, 2014, Russo et al., 2018]. Nonetheless, it is only until more recently that a series of work [Lu and Van Roy, 2019, Simchowitz et al., 2021] provides a through investigation into the influence of the algorithm's prior, and confirms the benefit of learning a meta-prior in bandits via both empirical and theoretical evidence [Cella et al., 2020, Basu et al., 2021, Kveton et al., 2021, Peleg et al., 2022]. The main difference between our work and the above is the use of a more complex prior, which also goes beyond the previously studied mixture prior [Hong et al., 2022b] and multi-layered Gaussian prior [Hong et al., 2022a]. On a slightly different note, a large corpus of work have investigated other ways to encode prior knowledge, including the use of arm hierarchy [Sen et al., 2021], graphs [Valko et al., 2014], or more commonly a latent parameter shared by the arms [Lattimore and Munos, 2014, Maillard and Mannor, 2014, Hong et al., 2020, Gupta et al., 2020].

Notation. All the variables are multi-dimensional unless otherwise specified. For a vector x, x^a represents the a-th coordinate of the vector, and x^2 represents its coordinate-wise square. A sequence of vectors $(x_l)_{l\in\{l_1,\dots,l_2\}}$ is written as $x_{l_1:l_2}$ for conciseness. $[n]$ denotes the sequence of integers $\{1,\dots,n\}$. To distinguish random variables from their instantiation, we represent the former with capital letters and the latter with the corresponding lowercase letters. Conditioning on $X = x$ is then abbreviated as $\cdot \mid x$. A Gaussian distribution centered at $\mu \in \mathbb{R}^d$ with covariance $\Sigma \in \mathbb{R}^{d\times d}$ is written as $\mathcal{N}(X;\mu,\Sigma)$ or simply $\mathcal{N}(\mu,\Sigma)$ if the random variable in question is clear from the context.

2 Preliminaries and Problem Description

In this section, we briefly review denoising diffusion models and introduce our meta-learning for bandits framework.

2.1 Denoising Diffusion Probabilistic Model

First introduced by Sohl-Dickstein et al. [2015] and recently popularized by Ho et al. [2020] and Song and Ermon [2019], denoising diffusion models (or the closely related score-based models) have demonstrated

state-of-the-art performance in various data generation tasks. A large number of variants of these models have been proposed since then. In this paper, we primarily follow the notation and formulation of Ho et al. [2020], with minor modifications to suit our purposes.

Intuitively speaking, diffusion models learn to approximate a distribution $\mathcal{Q}_0$ over $\mathbb{R}^d$ by training a series of denoisers with samples drawn from this distribution. Writing q for the probability density function (assume everything is Lebesgue measurable for simplicity) and X_0 for the associated random variable, we define the forward diffusion process with respect to a sequence of scale factors $(\alpha_\ell) \in (0,1)^L$ by

$$q(x_{1:L} \,|\, x_0) = \prod_{\ell=0}^{L-1} q(x_{\ell+1} \,|\, x_\ell), \qquad q(X_{\ell+1} \,|\, x_\ell) = \mathcal{N}(X_{\ell+1}; \sqrt{\alpha_{\ell+1}} x_\ell, (1-\alpha_{\ell+1}) I_d).$$

The first equality suggests that the forward process forms a Markov chain that starts at $x_0 \in \mathbb{R}^d$, while the second equality implies that the transition kernel is Gaussian. Further denoting the product of the scale factors by $\bar{\alpha}_\ell = \prod_{i=1}^{\ell} \alpha_i$, we then have $q(X_\ell \,|\, x_0) = \mathcal{N}(X_\ell; \sqrt{\bar{\alpha}_\ell} x_0, (1-\bar{\alpha}_\ell) I_d)$.

The sequence $(\alpha_\ell) \in (0,1)^L$ is chosen to be decreasing and such that $\bar{\alpha}_L \approx 0$. We thus expect $q(X_\ell) \approx \mathcal{N}(0, I_d)$. A denoising diffusion model learns to reverse the diffusion process by optimizing a certain parameter θ that defines a distribution $\mathcal{P}_\theta$ over random variables $X'_{0:L}$. The hope is that the marginal distribution $\mathcal{P}_\theta(X'_0)$ would be a good approximation of $\mathcal{Q}_0$. In practice, this is achieved by setting $p_\theta(X_\ell) = \mathcal{N}(0, I_d)$, enforcing the learned reverse process to be Markovian, and modeling $p_\theta(X_\ell \,|\, x_{\ell+1})$ as a Gaussian parameterized by[1]

$$\begin{aligned} p_\theta(X_\ell \,|\, x_{\ell+1}) &= q(X_\ell \,|\, x_{\ell+1}, X_0 = \underbrace{h_\theta(x_{\ell+1}, \ell+1)}_{\hat{x}_0}) \\ &= \mathcal{N}\left(X_\ell; \frac{\sqrt{\bar{\alpha}_\ell}(1-\alpha_{\ell+1})}{1-\bar{\alpha}_{\ell+1}} \hat{x}_0 + \frac{\sqrt{\alpha_{\ell+1}}(1-\bar{\alpha}_\ell)}{1-\bar{\alpha}_{\ell+1}} x_{\ell+1}; \frac{1-\bar{\alpha}_\ell}{1-\bar{\alpha}_{\ell+1}}(1-\alpha_{\ell+1}) I_d\right) \end{aligned} \tag{1}$$

In the above h_θ is the learned denoiser and $h_\theta(x_{\ell+1}, \ell+1)$ is the predicted clean sample.[2]

2.2 Meta-Learning of Bandit Tasks

Our work focuses on meta-learning problems in which the tasks are bandit instances drawn from an underlying distribution that we denote by $\mathcal{T}$. As in standard meta-learning, the goal is to learn an inductive bias from the meta training set that would improve the overall performance of an algorithm on new tasks drawn from the same distribution. In the context of this paper, the inductive bias is encoded in the form of a prior distribution that would be used by the Thompson sampling algorithm when the learner interacts with new bandit instances.

For the sake of simplicity, we restrict our attention to the multi-armed bandit scenario presented in Section 1, with the additional assumption that the noise in the rewards are Gaussian with known variance σ^2.[3] The only unknown information is thus the vector of the mean rewards $\mu = (\mu^a)_{a \in \mathcal{A}}$. For this specific situation, Thompson sampling takes as input a prior distribution over $\mathbb{R}^K$, samples a guess $\tilde{\mu}_t$ of the mean reward vector from the posterior distribution at each round, and pulls arm $a_t \in \arg\max_{a \in \mathcal{A}} \tilde{\mu}_t^a$ in that round. The posterior distribution itself is determined by both the prior and the interaction history, i.e., the sequence of the action-reward pairs $(a_s, r_s)_{s \in \{1,\dots,t-1\}}$.

As for the meta-training phase, we consider two situations that are distinguished by whether the learner has access to *perfect* data or not. In the former case, the meta-training set is composed of the exact means $\mathcal{D}_{\text{tr}} = \{\mu_B\}_B$ of training tasks B drawn from the distribution $\mathcal{T}$, whereas in the latter case the training set is

[1] With a slight abuse of notation, we drop the prime from $X'_{0:L}$ in the remaining of the work, but one should keep in mind that the distributions of $X_{0:L}$ induced by the forward process and of $X'_{0:L}$ modeled by the diffusion model are distinct.

[2] To obtain h_θ we typically train a neural network with a U-Net architecture. In [Ho et al., 2020], this network is trained to output the predicted noise $\bar{z}_\ell = (x_\ell - \sqrt{\bar{\alpha}_\ell} h_\theta(x_\ell, \ell))/\sqrt{1-\bar{\alpha}_\ell}$.

[3] We make this assumption as we are using diffusion prior. As far as we are aware, all the existing diffusion model posterior sampling algorithms for the case of Gaussian noise either rely on this assumption or circumvent it by adding some adjustable hyperparameter. How to extend these algorithms to cope with unknown noise variance properly is an interesting open question.

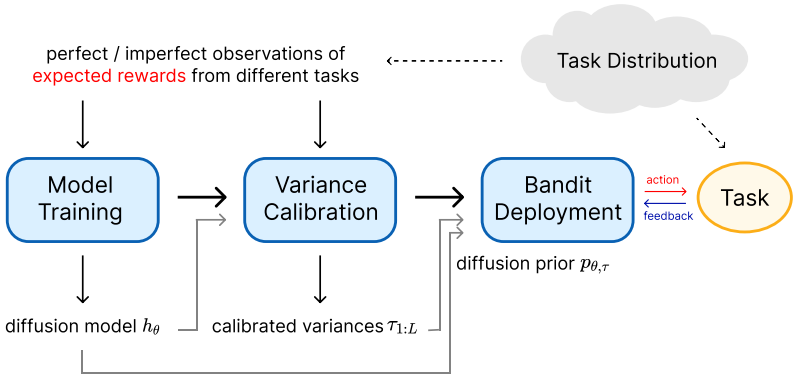

Figure 1: Overview of the meta-learning for bandits with diffusion prior framework.

composed of *incomplete and/or noisy* observations of these vectors (see Section 4 for details). We use the term *imperfect* data to informally refer to the scenario where the data is incomplete and/or noisy. The entire algorithm flow is summarized in Figure 1 and Algorithm 1, where both the model training and the variance calibration blocks together define the diffusion prior that is used by Thompson sampling in the deployment phase, as we will immediately see in Section 3.

Algorithm 1 Meta-learning for Bandits with Diffusion Models

1: `Meta-Training Phase a): Diffusion Model Training`
2: **Input:** Training set containing reward observations from different tasks
3: Train a diffusion model h_θ to model the distribution of the mean rewards (in case of imperfect data use Algorithm 5)
4: `Meta-Training Phase b): Variance Calibration`
5: **Input:** Diffusion model h_θ and calibration set containing reward observations from different tasks
6: Use Algorithm 2 to estimate the mean squared reconstruction errors $\tau_{1:L}$ of the model h_θ from different diffusion steps to calibrate the variance of each reverse step (in case of imperfect data use Algorithm 6)
7: `Meta-Deployment Phase`
8: **Input:** Diffusion model h_θ, reconstruction error $\tau_{1:L}$, and assumed noise level $\hat{\sigma}$
9: For any new task, run Thompson sampling with diffusion prior (Algorithm 4) with provided parameters

3 Using Trained Diffusion Models in Thompson Sampling

In this section, we describe how a learned diffusion model can be incorporated as a prior for Thompson sampling. For sake of presenting the core ideas, we focus here on the case where clean datasets $\mathcal{D}_{\text{tr}}$ and $\mathcal{D}_{\text{cal}}$ are used for training and calibration. The case where only imperfect datasets are available is addressed in Section 4. With a clean dataset $\mathcal{D}_{\text{tr}}$, diffusion model can be trained using well-known techniques, see e.g., [Ho et al., 2020]. Then, as outlined in Algorithm 1, given a trained model, the two remaining steps are: a) variance calibration, and b) Thompson sampling.

3.1 Variance Calibration

While Ho et al. [2020] fixed the variance of $p_\theta(X_\ell \,|\, x_{\ell+1})$ to that of $q(X_\ell \,|\, x_{\ell+1}, x_0)$ as expressed by Eq. (1), it was recently shown by Bao et al. [2021] that this choice was sub-optimal. This defect turns out to be critical when we use diffusion model as prior in online decision problems, as it falls short in quantifying the right level of uncertainty. To remedy this problem, we follow closely the approach of Bao et al. [2022] and calibrate the variances of the reverse process with a separate calibration set $\mathcal{D}_{\text{cal}}$. Precisely, we write

$$p_{\theta,\tau}(X_\ell \,|\, x_{\ell+1}) = \int q(X_\ell \,|\, x_{\ell+1}, x_0) p'_{\theta,\tau}(x_0 \,|\, x_{\ell+1})\, dx_0. \tag{2}$$

In the above, $p'_{\theta,\tau}(X_0 \,|\, x_{\ell+1})$ is a Gaussian distribution centered at the denoiser output $\hat{x}_0 = h_\theta(x_{\ell+1}, \ell+1)$ and $\tau = \tau_{1:L}$ is the optimized variance parameter. This is different from (1) where instead of $p'_{\theta,\tau}(x_0 \,|\, x_{\ell+1})dx_0$ we only have a Dirac concentrated at x_0. The covariance of $p'_{\theta,\tau}(X_0 \,|\, x_{\ell+1})$ is taken as the diagonal matrix $\mathrm{diag}(\tau^2_{\ell+1})$. As for the variance parameter $\tau_{\ell+1}$, it represents the (coordinate-wise) root mean squared reconstruction error and is computed on the calibration set $\mathcal{D}_{\mathrm{cal}}$ by constructing $\mathcal{D}_{\mathrm{cal},\ell}$ of pairs (x_0, x_ℓ) with $x_0 \in \mathcal{D}_{\mathrm{cal}}$ and x_ℓ sampled from $X_\ell \,|\, x_0$, and setting

$$\tau^a_\ell = \sqrt{\sum_{x_0, x_\ell \in \mathcal{D}_{\mathrm{cal},\ell}} \|x^a_0 - h^a_\theta(x_\ell, \ell)\|^2 / \operatorname{card}(\mathcal{D}_{\mathrm{cal},\ell})}.$$

The above procedure is summarized in Algorithm 2. Intuitively, the calibration step automatically adjusts how much we rely on the learned model in the upcoming tasks by taking the reconstruction error as a proxy for the model's quality. We opt for a simple model here in which the covariance matrix is the same at all points, whereas Bao et al. [2022] fit a neural network to predict the mean squared residual at every x_ℓ. Once the reconstruction errors are computed, the covariance of $p_{\theta,\tau}$ can be derived from (2).

Algorithm 2 Diffusion Model Variance Calibration

Input: Diffusion model h_θ, calibration set $\mathcal{D}_{\mathrm{cal}} = \{x_{i,0}\}_i$, noise standard deviation σ
Output: Reconstructions errors $\tau_{1:L}$
for $\ell = 1 \dots L$ **do**
    Construct $\mathcal{D}_{\mathrm{cal},\ell} = \{x_{i,0}, x_{i,\ell}\}_i$ by sampling $x_{i,\ell}$ from $X_\ell \,|\, x_{i,0}$
    for $a = 1 \dots K$ **do**
        Set $\tau^a_\ell \leftarrow \sqrt{\sum_{x_0, x_\ell \in \mathcal{D}_{\mathrm{cal},\ell}} \|x^a_0 - h^a_\theta(x_\ell, \ell)\|^2 / \operatorname{card}(\mathcal{D}_{\mathrm{cal},\ell})}$
    end for
end for

3.2 Thompson Sampling with Diffusion Prior

We next proceed to discuss how to perform Thompson sampling with a diffusion model learned prior $p_{\theta,\tau}$. For this, we need to sample from the posterior when the prior is specified as such. Concretely, for a given evidence y_0 of x_0 with known $q(y_0 \,|\, x_0)$, we are interested in sampling from $X_0 \,|\, y_0$. While an exact solution does not exist in general, we may look at this problem as sampling from the prior mixed with evidence y_0. In this regard, our algorithm gradually guides the sample towards the evidence during the sampling process. This is achieved by conditioning the reverse Markovian process on $Y_0 = y_0$ and seeks an approximation for each conditional reverse step.

In the case of multi-armed bandits, $y_0 = (a_s, r_s)_{s \in \{1,\dots,t\}}$ is the interaction history and $x_0 = \mu \in \mathbb{R}^K$ is the mean reward vector of the task, and it holds that

$$q(y_0 \,|\, x_0) \propto \prod_{s=1}^{t} q(r_s \,|\, \mu, a_s) = \prod_{s=1}^{t} \mathcal{N}(r_s; \mu^{a_s}, \sigma^2) \quad \text{[as a function of } x_0\text{]}. \tag{3}$$

By the proportionality we hide all the randomness in the learner's actions. This is legitimate because the learner's actions only depend on the mean reward vector via their interaction history with the environment, i.e., $q(a_s \,|\, a_1, r_1, \dots, a_{s-1}, r_{s-1}, \mu) = q(a_s \,|\, a_1, r_1, \dots, a_{s-1}, r_{s-1})$. The initialization and the recursive steps of our conditional sampling scheme tailored to this situation is then provided below. Detailed derivation behind the algorithm is provided in Appendix A.1.

Sampling from $X_L \,|\, y_0$. For this part, we simply ignore y_0 and sample from $\mathcal{N}(0, I_d)$ as before.

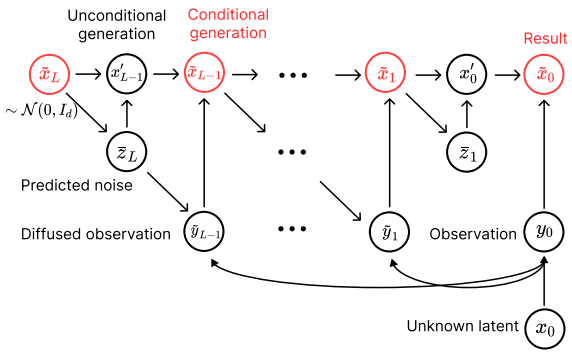

Figure 2: Illustration of the proposed posterior sampling with diffusion prior algorithm (Algorithm 3).

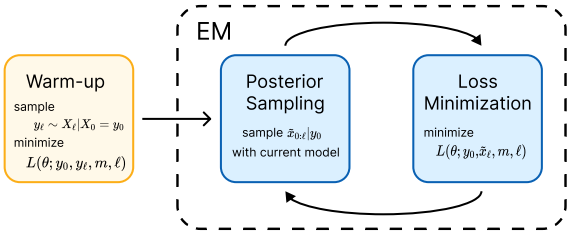

Figure 3: Overview of the proposed training procedure to deal with incomplete and/or noisy data.

Sampling from $X_\ell \,|\, x_{\ell+1}, y_0$ We first create an *unconditional* latent variable x'_ℓ by sampling from the unconditional reverse process $p_{\theta,\tau}(X_\ell \,|\, x_{\ell+1})$. We then perform coordinate-wise operation by distinguishing between the following two situations.

- Arm a has never been pulled in the first t rounds: In this case we just set x_ℓ^a to be $x_\ell'^a$.
- Arm a has been pulled in the first t rounds: We denote by $\hat{\mu}_t^a = \sum_{s=1}^t r_s \mathbb{1}\{a_s = a\}/N_t^a$ as the empirical mean and $\sigma_t^a = \sigma/\sqrt{N_t^a}$ as the adjusted standard deviation, where N_t^a is the number of times that arm a has been pulled up to time t (included). We also write $\zeta_{\ell,1}^a$ for the standard deviation of $p_{\theta,\tau}(X_\ell^a \,|\, x_{\ell+1})$ and define the diffused observation

$$\tilde{y}_\ell^a = \sqrt{\bar{\alpha}_\ell}\hat{\mu}_t^a + \sqrt{1-\bar{\alpha}_\ell}\bar{z}_{\ell+1}^a + \zeta_{\ell,2}^a \tilde{z}_{\ell+1}^a \tag{4}$$

that contains a predicted noise component $\bar{z}_{\ell+1}$ satisfying $x_{\ell+1} = \sqrt{\bar{\alpha}_{\ell+1}} h_\theta(x_{\ell+1}, \ell+1) + \sqrt{1-\bar{\alpha}_{\ell+1}}\bar{z}_{\ell+1}$ and an independent noise component with $\tilde{z}_{\ell+1}^a$ sampled from $\mathcal{N}(0,1)$ and further multiplied by

$$\zeta_{\ell,2}^a = \sqrt{\bar{\alpha}_\ell \left((\sigma_t^a)^2 + \frac{\bar{\alpha}_{\ell+1}(1-\bar{\alpha}_\ell)}{\bar{\alpha}_\ell(1-\bar{\alpha}_{\ell+1})} (\tau_{\ell+1}^a)^2 \right)}. \tag{5}$$

The output of the conditional reverse step is then a weighted sum of the diffused observation and the unconditional latent variable[4][5]

$$x_\ell^a = \frac{(\zeta_{\ell,1}^a)^{-2} x_\ell'^a + (\zeta_{\ell,2}^a)^{-2} \tilde{y}_\ell^a}{(\zeta_{\ell,1}^a)^{-2} + (\zeta_{\ell,2}^a)^{-2}}.$$

As we see above, while the case of single observation with missing entries is clearly a special case of bandit observations, in terms of algorithmic scheme, it becomes equivalent when we summarize the interaction history of bandits with mean $\hat{\mu}_t^a$ and standard deviation σ_t. Therefore, we present the posterior sampling algorithm for the former situation in Algorithm 3, and depict the induced Thompson sampling algorithm in Algorithm 4. It is also important to note that while our algorithms shares similarity with existing posterior sampling methods [Song et al., 2021, Chung et al., 2022b], we supplement our diffused observation $\tilde{y}_\ell^a$ with a predicted noise component that improves the coherence between the observation and the generated sample.

4 Training Diffusion Models from Imperfect Data

Standard training procedure of diffusion models require access to a dataset of clean samples $\mathcal{D}_{\text{tr}} = \{x_{i,0}\}_{i\in[n]}$. Nonetheless, in most bandit applications, it is nearly impossible to obtain such dataset as the exact mean

[4] We set $x_\ell^a = \tilde{y}_\ell^a$ if $\zeta_{\ell,2}^a = 0$.

[5] The weighted average is also equivalent to sampling x_ℓ^a from a certain Gaussian distribution; see Appendix A.1 for details.

Algorithm 3 Posterior Sampling with Diffusion Prior

Input: Observation $y_0 \in \mathbb{R}^K$, noise standard deviation $\sigma \in \mathbb{R}^K$, binary mask $m \in \{0,1\}^K$, diffusion model h_θ and associated reconstruction errors $\tau_{1:L}$
Output: Posterior sample x_0 (resp. $x_{0:L}$) approximately sampled from $X_0 \,|\, y_0$ (resp. $X_{0:L} \,|\, y_0$)
Sample $x_L \sim \mathcal{N}(0, I_d)$
for $\ell \in L-1, \dots, 0$ **do**
  Predict clean sample $\hat{x}_0 \leftarrow h_\theta(x_{\ell+1}, \ell+1)$ and associated noise $\bar{z}_{\ell+1}$
  Sample unconditional latent variable x_ℓ from $p_{\theta,\tau}(X_\ell \,|\, x_{\ell+1})$
  for $a \in \mathcal{A}$ such that $m^a = 1$ **do**
    Sample $\tilde{z}^a_{\ell+1} \sim \mathcal{N}(0,1)$ and compute $\zeta^a_{\ell,2}$ following (5)
    Compute diffused observation $\tilde{y}^a_\ell \leftarrow \sqrt{\bar{\alpha}_\ell} y^a_0 + \sqrt{1-\bar{\alpha}_\ell}\bar{z}^a_{\ell+1} + \zeta^a_{\ell,2}\tilde{z}^a_{\ell+1}$
    Set $x^a_\ell \leftarrow \frac{(\zeta^a_{\ell,1})^{-2} x^a_\ell + (\zeta^a_{\ell,2})^{-2}\tilde{y}^a_\ell}{(\zeta^a_{\ell,1})^{-2} + (\zeta^a_{\ell,2})^{-2}}$ ▷ $\zeta^a_{\ell,1}$ is the standard deviation of $p_{\theta,\tau}(X^a_\ell \,|\, x_{\ell+1})$
  end for
end for

Algorithm 4 Thompson Sampling with Diffusion Prior (DiffTS)

Input: Diffusion model h_θ, reconstruction errors $\tau_{1:L}$, assumed noise level $\hat{\sigma} \in \mathbb{R}$
for $t = 1, \dots$ **do**
  Sample $\tilde{x}_0$ using Algorithm 3 with $y_0 \leftarrow \hat{\mu}_{t-1}$, $\sigma \leftarrow \sigma_{t-1}$, m defined by $m^a = \mathbb{1}\{N^a_{t-1} > 0\}$
  Pull arm $a_t \in \arg\max_{a \in \mathcal{A}} \tilde{x}^a_0$
  Update number of pulls N^a_t, scaled standard deviation σ^a_t, and empirical reward $\hat{\mu}^a_t$ for $a \in \mathcal{A}$
end for

reward vector μ of each single task is never directly observed. Instead, one can collect imperfect observations of these vectors, either through previous bandit interactions or forced exploration. Taking this into account, in this section, we build towards a systematic procedure to train (and calibrate) diffusion models from imperfect (incomplete and/or noisy) data. It is worth noticing that the application scope of our methodology goes beyond the bandit setup and covers any situation where imperfect data are available. As an example, we apply our approach to train from imperfect images (corrupted MNIST and Fashion-MNIST [Xiao et al., 2017] datasets) and obtain promising results (details are provided in Appendix D.3).

Setup. For ease of exposition, we first focus on the case of uniform noise variance. Extension to deal with non-uniform noise variance is later presented in Remark 1. When all the observed noises have the same variance $\sigma^2 \in \mathbb{R}$, the samples of the imperfect dataset $\check{\mathcal{D}}_{\text{tr}} = \{y_{i,0}\}_{i\in[n]}$ can be written as $y_{i,0} = m_i \odot (x_{i,0} + z_i)$ where $m_i \in \{0,1\}^K$ is binary mask, z_i is a noise vector sampled from $\mathcal{N}(0, \sigma^2 I_d)$, and $\odot$ denotes element-wise multiplication.[6] In the considered bandit problem, such dataset can be obtained by randomly pulling a subset of arms once for each arm. We also assume that the associated masks $\{m_i\}_{i\in[n]}$ and the noise standard deviation σ are known. We can thus rewrite the dataset as $\check{\mathcal{D}}_{\text{tr}} = \{y_{i,0}, m_i\}_{i\in[n]}$.

4.1 Training with Imperfect Data

In presence of perfect data, diffusion model training optimizes the denoising objective

$$\mathbb{E}_{\ell \sim \text{Uniform}(\{1,\dots,L\}), x_0 \sim \mathcal{Q}_0, x_\ell \sim X_\ell \,|\, x_0}[\|x_0 - h_\theta(x_\ell, \ell)\|^2]. \tag{6}$$

Nonetheless, neither x_0 nor x_ℓ are available when we only have access to an imperfect dataset $\check{\mathcal{D}}_{\text{tr}}$. To tackle these challenges, we propose an expectation-maximization (EM)-type procedure where in the place of the expectation step we perform sampling of latent variables and in the place of the maximization step we

[6] As we will see Remark 1, the masking of an entry can also be viewed as an observation with infinite variance.

minimize a tailored loss function. An indicative algorithmic scheme is summarized in Algorithm 5 (without mini-batching, dataset shuffling, and the use of specific optimization algorithm).

Posterior Sampling. Due to the absence of a clean observation of x_0, it is impossible to sample x_ℓ via the forward diffusion process. Nonetheless, we can perform posterior sampling with the current model as done in several variants of stochastic EM [Fort and Moulines, 2003]. In fact, as explained in Section 2.1, a diffusion model can be regarded as a probability model over the random variables $X_{0:L}$. A typical expectation step in EM for a given parameter θ' requires us to compute the expected log likelihood function

$$Q(\theta) = \sum_{i=1}^{n} \mathbb{E}_{X_{i,0:L} \,|\, y_{i,0}, m_i, \theta'} \log p_\theta(X_{i,0:L}).$$

Nonetheless, this is intractable in general due to the use of neural network in the definition of p_θ. To circumvent this issue, we can instead sample $\tilde{x}_{i,0:L}$ from the posterior with density $p_{\theta'}(\cdot \,|\, y_{i,0}, m_i)$ and use stochastic gradient ascent to maximize the log likelihood function.

Loss Minimization. Having obtained the posterior samples, we have the option to either maximize the log-likelihood of $\widetilde{\mathcal{D}}_{\text{tr}}$ or minimize the denoising loss $\sum_{\tilde{x}_{0:L} \in \widetilde{\mathcal{D}}_{\text{tr}}} \sum_{\ell=1}^{L} \|\tilde{x}_0 - h_\theta(\tilde{x}_\ell, \ell)\|^2$. However, both of these approaches heavily rely on the samples generated in the posterior sampling step, which can bias the model towards generating low-quality samples during early stages of training. To address this issue, we propose to consider a loss function that utilizes the actual observation y_0 and not the reconstructed sample $\tilde{x}_0$. Fix a small value ε and a regularization parameter λ, the new loss function for a sample pair $(y_0, \tilde{x}_\ell)$ at diffusion step ℓ with associated mask m is defined as

$$L(\theta; y_0, \tilde{x}_\ell, m, \ell) = \|m \odot y_0 - m \odot h_\theta(\tilde{x}_\ell, \ell)\|^2 + 2\lambda \sqrt{\bar{\alpha}_\ell} \sigma^2 \, \mathbb{E}_{b \sim \mathcal{N}(0,I)} \, b^\top \left(\frac{h_\theta(\tilde{x}_\ell + \varepsilon b, \ell) - h_\theta(\tilde{x}_\ell, \ell)}{\varepsilon} \right). \quad (7)$$

The above loss function is composed of two components that address respectively the incompleteness and the noise in the observations. First, it handles incomplete (missing) data by only considering the observed entries as determined by the element-wise product with the mask in the first term. Next, to account for noise, we include a regularization term that penalizes the denoiser from varying too much when the input changes. Overall, our denoising loss find its roots in a series of work [Metzler et al., 2018, Zhussip et al., 2019] that investigates the training of denoiser in the absence of ground-truth clean data. In particular, the expectation here is an approximation of the divergence $\operatorname{div}_{\tilde{x}_\ell}(h_\theta(\tilde{x}_\ell, \ell))$ that appears in Stein's unbiased risk estimate (SURE) [Stein, 1981, Eldar, 2008], an unbiased estimator of the mean squared error whose computation only requires the use of noisy samples.[7]

From a practical viewpoint, the regularization term provides a trade-off between the bias and the variance of the learned model. When λ is set to 0, the model learns to generate noisy samples, which corresponds to a flatter prior that encourages exploration. When λ gets larger, the model tries to denoise from the observed noisy samples. This can however deviate the model from the correct prior and accordingly jeopardize the online learning procedure.

Overall Procedure. The complete algorithm for training from imperfect data is presented in Algorithm 5. It alternates between the posterior sampling and the loss minimization steps. While any posterior sampling algorithm can be used for the former, in our experiments we simply rely on the one presented in Section 3.2 (note that we actually sample the entire chain $\tilde{x}_{0:L}$ in the procedure of sampling $\tilde{x}_0$) to acquire posterior samples $\widetilde{\mathcal{D}}_{\text{tr}} = \{\tilde{x}_{i,0:L}\}_{i \in \mathcal{S} \subseteq [n]}$ for (a subset of) the dataset. Then, in the loss minimization step we sample from the dataset $\widetilde{\mathcal{D}}'_{\text{tr}} = \{\tilde{x}_{i,0:L}, y_{i,0}, m_i\}_{i \in \mathcal{S}}$ and use stochastic gradient descent to minimize $\sum_{(\tilde{x}_{0:L}, y_0, m) \in \widetilde{\mathcal{D}}'_{\text{tr}}} \sum_{\ell=1}^{L} L(\theta; y_0, \tilde{x}_\ell, m, \ell)$. Moreover, we begin with a warm-up phrase where we sample

[7] When $\lambda = 1$, $x_\ell = \tilde{x}_\ell = \sqrt{\bar{\alpha}_\ell} y_0$, $m = \mathbf{1}$ (i.e., all the entries are observed), and the expectation is replaced by the divergence, we recover SURE up to additive constant $-K\sigma^2$. See Appendix A.2 for details.

Algorithm 5 Diffusion Model Training from Imperfect (Incomplete and/or Noisy) Data

Input: Training set $\check{\mathcal{D}}_{\text{tr}} = \{y_{i,0}, m_i\}_i$, calibration set $\check{\mathcal{D}}_{\text{cal}}$, noise standard deviation σ, number of warm-up, outer, and inner training steps S, J, and S'
Output: Diffusion model h_θ
`Warm-up`
for $s = 1, \ldots, S$ **do**
  Sample y_0, m from $\check{\mathcal{D}}_{\text{tr}}$
  Sample ℓ from the uniform distribution over $\{1, ..., L\}$
  Sample y_ℓ from $X_\ell \,|\, X_0 = y_0$
  Take gradient step to minimize $L(\theta; y_0, y_\ell, m, \ell)$ (Eq. (7))
end for
`Main Training Procedure`
for $j = 1, \ldots, J$ **do**
  `Posterior Sampling`
  Compute reconstructions errors $\tau_{1:L}$ with Algorithm 6 using $\check{\mathcal{D}}_{\text{cal}}$
  Construct $\widetilde{\mathcal{D}}'_{\text{tr}} = \{\tilde{x}_{i,0:L}, y_{i,0}, m_i\}_i$ with Algorithm 3
  `Loss Minimization`
  for $s = 1, \ldots, S'$ **do**
    Sample $\tilde{x}_{0:L}, y_0, m$ from $\check{\mathcal{D}}_{\text{tr}}$
    Sample ℓ from the uniform distribution over $\{1, ..., L\}$
    Take gradient step to minimize $L(\theta; y_0, \tilde{x}_\ell, m, \ell)$ (Eq. (7))
  end for
end for

$y_\ell = \sqrt{\bar{\alpha}_\ell} y_0 + \sqrt{1 - \bar{\alpha}_\ell}\tilde{z}_\ell$ with $\tilde{z}_\ell$ sampled from $\mathcal{N}(0, I_d)$ as in standard diffusion model training but replace the mean squared error by the loss function L introduced in (7).[8] This initial phase produces better training samples than posterior sampling with randomly initialized model.

Remark 1 (Bandit observations / observations with varying variances)**.** When the observations come from bandit interactions and each arm can be pulled more than once, we can first summarize the interaction history by the empirical mean and the vector of adjusted standard deviation as suggested in Section 3.2. Therefore, it remains to address the case where the noise vector z_i is sampled from $\mathcal{N}(0, \text{diag}({\sigma_i}^2))$ for some vector $\sigma_i \in \mathbb{R}^K$. As the design of our posterior sampling algorithm already takes this into account, the posterior sampling steps of the algorithm remains unchanged. The only difference would thus lie in the definition of the modified loss (7). Intuitively, we would like to give more weights to samples that are less uncertain. This can be achieved by weighting the loss by the inverse of the variances, that is, we set

$$L'(\theta; y_0, \tilde{x}_\ell, m, \sigma, \ell) = \sum_{a=1}^{K} \frac{m^a |y_0^a - h_\theta^a(\tilde{x}_\ell, \ell)|}{(\sigma^a)^2} + 2\lambda\sqrt{\bar{\alpha}_\ell}\, \mathbb{E}_{b\sim\mathcal{N}(0,I)}\, b^\top \left(\frac{h_\theta(\tilde{x}_\ell + \varepsilon b, \ell) - h_\theta(\tilde{x}_\ell, \ell)}{\varepsilon} \right). \quad (8)$$

To make sure the above loss is always well defined, we may further replace $(\sigma^a)^2$ by $(\sigma^a)^2 + \delta$ for some small $\delta > 0$. It is worth noticing that one way to interpret the absence of observation $m^a = 0$ is to set the corresponding variance to infinite, i.e., $\sigma^a = +\infty$. In this case we see there is even no need of m anymore as the coordinates with $\sigma^a = +\infty$ would already be given 0 weight. Finally, to understand why we choose to weight with the inverse of the variance, we consider a scalar x, and a set of noisy observations $y_1, \ldots, y_n$ respectively drawn from $\mathcal{N}(x, \sigma_1^2), \ldots, \mathcal{N}(x, \sigma_n^2)$. Then, the maximum likelihood estimate of x is $\sum_{i=1}^n \sigma_i^2 y_i / (\sum_{i=1}^n \sigma_i^2)$.

[8] In our experiments, we impute the missing values of y_0 by a non-zero constant.

4.2 Variance Calibration with Imperfect Data

As mentioned in Section 3.1, a reliable variance estimate of the reverse process is essential for building a good diffusion prior. This holds true not only for the online learning process at test phase, but also for the posterior sampling step of our training procedure. The algorithm introduced in Section 3.1 calibrates the variance through perfect data. In this part, we extend it to operate with imperfect data.

Let $\check{\mathcal{D}}_{\text{cal}}$ be a set of imperfect data constructed in the same way as $\check{\mathcal{D}}_{\text{tr}}$. We write $\check{\mathcal{D}}_{\text{cal}}^a = \{(y_0, m) \in \check{\mathcal{D}}_{\text{cal}} : m^a = 1\}$ as the subset of $\check{\mathcal{D}}_{\text{cal}}$ for which a noisy observation of the feature at position a is available. Our algorithm (outlined in Algorithm 6) is inspired by the following two observations. First, if the entries are missing completely at random, observed y_0^a of $\check{\mathcal{D}}_{\text{cal}}^a$ and sampled $x_0^a + z^a$ with $x_0 \sim \mathcal{Q}_0$ and $z \sim \mathcal{N}(0, \sigma^2 I)$ have the same distribution. Moreover, for any triple (x_0, y_0, x_ℓ) with $y_0 = x_0 + z$, $x_\ell = \sqrt{\bar{\alpha}_\ell} x_0 + \sqrt{1 - \bar{\alpha}_\ell} \bar{z}_\ell$ and x_0, z, and $\bar{z}_\ell$ sampled independently from $\mathcal{Q}_0$, $\mathcal{N}(0, \sigma^2 I)$, and $\mathcal{N}(0, I)$, it holds that

$$\mathbb{E}[\|y_0^a - h_\theta^a(x_\ell, \ell)\|^2] = \mathbb{E}[\|x_0^a - h_\theta^a(x_\ell, \ell)\|^2] + \sigma^2.$$

We can thus estimate $\mathbb{E}[\|x_0^a - h_\theta^a(x_\ell, \ell)\|^2]$ if we manage to pair each $y_0^a \in \check{\mathcal{D}}_{\text{cal}}^a$ with a such x_ℓ.

We again resort to Algorithm 3 for the construction of x_ℓ (referred to as $\tilde{x}_\ell$ in Algorithm 6 and hereinafter). Unlike the training procedure, here we first construct $\tilde{x}_0$ and sample $\tilde{x}_\ell$ from $X_\ell \,|\, \tilde{x}_0$ to decrease the mutual information between $\tilde{x}_\ell$ and y_0. Nonetheless, the use of our posterior sampling algorithm itself requires a prior with calibrated variance. To resolve the chicken-and-egg dilemma, we add a warm-up step where we precompute the reconstruction errors with Algorithm 2 by treating $\check{\mathcal{D}}_{\text{cal}}$ as the perfect dataset. In our experiments, we observe this step yields estimates of the right order of magnitude but not good enough to be used with Thompson sampling, while the second step brings the relative error to as small as 5% compare to the estimate obtained with perfect validation data using Algorithm 2.

Algorithm 6 Diffusion Model Variance Calibration from Imperfect (incomplete and/or noisy) Data

Input: Diffusion model h_θ, calibration set $\check{\mathcal{D}}_{\text{cal}} = \{y_{i,0}, m_i\}_i$, noise standard deviation σ
Output: Reconstructions errors $\tau_{1:L}$
`Data Set Preprocessing`
Precompute reconstructions errors $\tau_{1:L}$ with Algorithm 2 and $\mathcal{D}_{\text{cal}} \leftarrow \check{\mathcal{D}}_{\text{cal}}$ (masks ignored)
Construct $\widetilde{\mathcal{D}}_{\text{cal}} = \{\tilde{x}_{i,0}, y_{i,0}, m_i\}_i$ with Algorithm 3
`Variance Calibration`
for $\ell = 1 \dots L$ **do**
    Construct $\widetilde{\mathcal{D}}_{\text{cal},\ell} = \{\tilde{x}_{i,\ell}, y_{i,0}, m_i\}_i$ by sampling $\tilde{x}_{i,\ell}$ from $X_\ell \,|\, \tilde{x}_{i,0}$
    for $a = 1 \dots K$ **do**
        Let $\widetilde{\mathcal{D}}_{\text{cal},\ell}^a = \{\tilde{x}_\ell, y_0 : (\tilde{x}_\ell, y_0, m) \in \widetilde{\mathcal{D}}_{\text{cal},\ell}, m^a = 1\}$
        Set $\tau_\ell^a \leftarrow \sqrt{(\sum_{\tilde{x}_\ell, y_0 \in \widetilde{\mathcal{D}}_{\text{cal},\ell}^a} \|x_0^a - h_\theta^a(x_\ell, \ell)\|^2 / \operatorname{card}(\widetilde{\mathcal{D}}_{\text{cal},\ell}^a)) - \sigma^2}$
    end for
end for

5 Numerical Experiments

In this section, we illustrate the benefit of using diffusion prior through numerical experiments on both real and synthetic data. Missing experimental details, ablation studies, and additional experiments are presented in Appendices B to D.

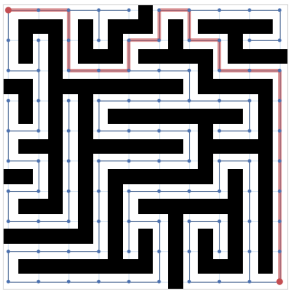

Figure 4: An example task of the `2D Maze` problem presented below. The red path indicates the optimal (super-)arm.

Problem Construction. To demonstrate the wide applicability of our technique, we consider here three bandit problems respectively inspired by the applications in recommendation

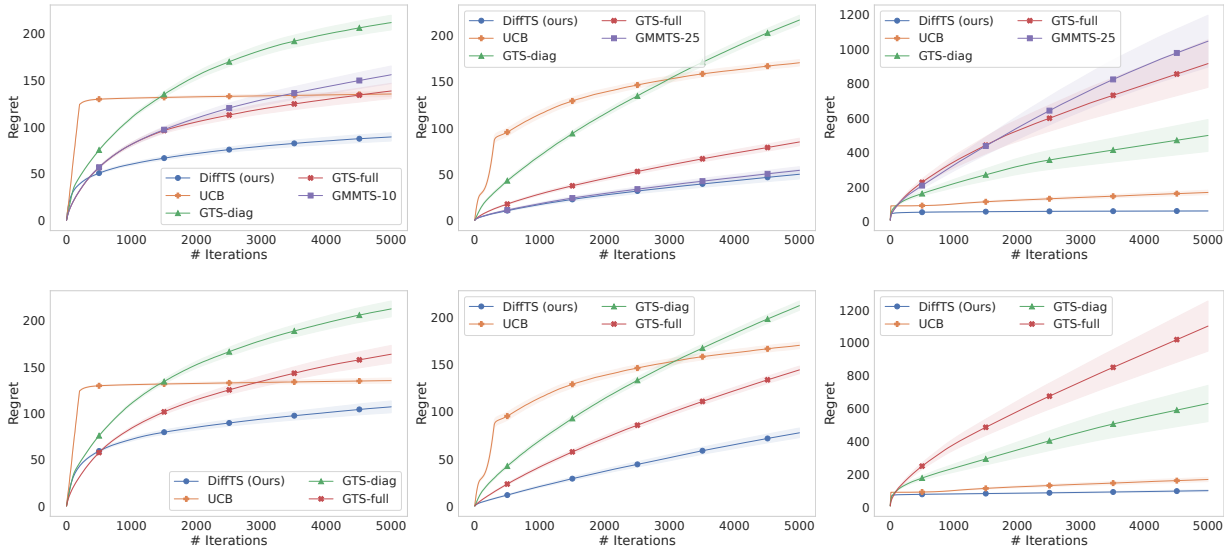

(a) `Popular and Niche` **(b)** `iPinYou Bidding` **(c)** `2D Maze`

Figure 5: Regret performances on three different problems with priors fitted/trained on either exact expected rewards (top) or partially observed noisy rewards (bottom). The results are averaged over tasks of a test set and shaded areas represent standard errors.

system, online pricing, and online shortest path routing. Detailed description of the problems and some visualization that help understand the problem structures are provided in Appendices B.1 and E. The first and the third problems listed below rely on synthetic data, where we only specify the construction of the means and the rewards are obtained by perturbing the means with Gaussian noise of standard deviation $\sigma = 0.1$, and for the second problem we use the iPinYou dataset [Liao et al., 2014].

1. `Popular and Niche` Problem. We consider here the problem of choosing items to recommend to customers. Let $K = 200$. The arms (items) are separated into 40 groups, each of size 5. Among these, 20 groups of arms correspond to the popular items and tend to have high mean rewards. However, these arms are never the optimal ones. The other 20 groups of arms correspond to the niche items. Most of them have low mean rewards but a few of them (those that match the preferences of the customer) have mean rewards that are higher than that of all the other arms.

2. `iPinYou Bidding` Problem. We consider here the problem of setting the bid price in auctions. Let $v = 300$ be the value of the item. Each arm corresponds to a bid price $b \in \{0, ..., 299\}$, and the reward is either $v - b$ when the learner wins the auction or 0 otherwise. The reward distribution of a task is then solely determined by the winning rates which are functions of the learner's bid and the distribution of the highest bid from competitors. For the latter we use the corresponding empirical distributions of 1352 ad slots from the iPinYou bidding data set [Liao et al., 2014] (each ad slot is a single bandit task).

3. `2D Maze` Problem. We consider here an online shortest path routing problem on grid graphs. We formalize it as a reward maximization combinatorial bandit with semi-bandit feedback. As shown in Figure 4, the supers arms are the simple paths between the source and the destination (fixed across all the tasks) whereas the base arms are the edges of the grid graph. At each round, the learner picks a super arm and observes the rewards of all the base arms (edges) that are contained in the super arm (path). Moreover, the edges' mean rewards in each task are derived from a certain 2D maze. The mean reward is -1 when there is a wall on the associated case (marked by the black color) and -0.01 otherwise.

Training, Baselines, and Evaluation. To train the diffusion models, for each problem we construct a training set $\mathcal{D}_{\text{tr}}$ and a calibration set $\mathcal{D}_{\text{cal}}$ that contain the expected means of the tasks. We then conduct experiments for the following two configurations:

1. Learn from perfect data: The priors are learned using $\mathcal{D}_{\text{tr}}$ and $\mathcal{D}_{\text{cal}}$ that contain the exact mean rewards. Standard training procedure is applied here.

2. Learn from imperfect data: The priors are learned using $\check{\mathcal{D}}_{\text{tr}}$ and $\check{\mathcal{D}}_{\text{cal}}$ that are obtained from $\mathcal{D}_{\text{tr}}$ and $\mathcal{D}_{\text{cal}}$ by perturbing the samples with noise of standard deviation 0.1 and then dropping each feature of a sample with probability 0.5. To tackle this challenging situation we adopt the approach proposed in Section 4.

In terms of bandit algorithms, we compare our method, DiffTS, with UCB, Thompson sampling with Gaussian prior using either diagonal or full covariance matrix (GTS-diag and GTS-full), and Thompson sampling with Gaussian mixture prior [Hong et al., 2022b] with either 10 or 25 components (GMMTS-10 and GMMTS-25).[9] These priors are also learned with the same perfect / imperfect data that we use to train diffusion models. We however skip the GMM baseline for the imperfect data setup because we are not able to find any existing algorithm that is able to learn a good GMM on the imperfect data that we consider here.

The performance of the algorithms are then evaluated by their average regret on a standalone test set— for a sequence of arms $(a_t)_{t\in\{1,\dots,T\}}$ pulled by an algorithm in a bandit task, the induced regret is $\text{Reg}_T = T\mu^{a^\star} - \sum_{t=1}^{T} \mu^{a_t}$, where $a^\star \in \arg\max_{a\in\mathcal{A}} \mu^a$ is an optimal arm in this task. The assumed noise level $\hat{\sigma}$ is fixed to the same value across all the methods

Results. The results are presented in Figure 5. For ease of readability, among the two GMM priors (10 and 25 components), we only show the one that achieves smaller regret. We see clearly that throughout the three problems and the two setups considered here, the proposed DiffTS algorithm always has the best performance. The difference is particularly significant in the `Popular and Niche` and `2D Maze` problems, in which the regret achieved by DiffTS is around two times smaller than that achieved by the best performing baseline method. This confirms that using diffusion prior is more advantageous in problems with complex task distribution.

On the other hand, we also observe that the use of GMM prior in these two problems leads to performance worse than that of GTS-full, whereas it yields performance that is as competitive as DiffTS in the iPinYou Bidding problem. This is coherent with the visualizations we make in Appendix E, which shows that the fitted GMM is only capable of generating good samples in the `iPinYou Bidding` problem. This, however, also suggests that the use of a more complex prior is a double-edged sword, and can lead to poor performance when the data distribution is not faithfully represented.

In Appendix C, we further present ablation studies to investigate the impacts of various components of our algorithm. In summary, we find out both the variance calibration step and the EM-like procedure for training with imperfect data are the most crucial to our algorithms, as dropping either of the two could lead to severe performance degradation. We also affirm that the use of SURE-based regularization does lead to smaller regret, but finding the optimal regularization parameter λ is a challenging problem.

Finally, while the good performance of DiffTS is itself an evidence of the effectiveness of our sampling and training algorithms, we provide additional experiments in Appendix D to show how these methods can actually be relevant in other contexts.

6 Concluding Remarks

In this work, we argue that the expressivity and flexibility of diffusion models make them a promising choice for representing complex priors in real-world online decision making problems. Through numerical experiments, we demonstrate that using a diffusion prior in combination with a proposed Thompson sampling algorithm can significantly reduce the achieved regret in multi-armed bandit problems. Additionally, we propose a training procedure for diffusion models that can handle imperfect training data, addressing a common issue in bandit scenarios, and could be applicable elsewhere too.

[9] For the `2D Maze` problem we consider their combinatorial extensions in which the UCB index / sampled mean of a super arm is simply the sum of the corresponding quantities of the contained base arms.

Looking ahead, our work raises a number of exciting but challenging research questions. One potential extension is to apply our approach to meta-learning problems in contextual bandits or reinforcement learning. This would involve modeling a distribution of functions or even Markov decision processes by diffusion models, which remains a largely unexplored area despite a few attempts that work toward these purposes [Dutordoir et al., 2022, Nava et al., 2022]. Another factor we did not address in our work is the uncertainty of the learned model itself (in contrast to the uncertainty modeled by the model). When the diffusion model is trained on a limited amount of data, its uncertainty is high, and using it as a fixed prior may lead to poor results. Finally, the posterior sampling algorithm for the diffusion model is a key bottleneck in terms of scaling our method. There has been significant work on accelerating unconditional sampling of diffusion models [Salimans and Ho, 2021, Dockhorn et al., 2022, Zheng et al., 2022], but it is still an open question how to incorporate these techniques into posterior sampling schemes.

References

Anurag Ajay, Yilun Du, Abhi Gupta, Joshua Tenenbaum, Tommi Jaakkola, and Pulkit Agrawal. Is conditional generative modeling all you need for decision-making? *arXiv preprint arXiv:2211.15657*, 2022.

Peter Auer. Using confidence bounds for exploitation-exploration trade-offs. *Journal of Machine Learning Research*, 3(Nov):397–422, 2002.

Fan Bao, Chongxuan Li, Jun Zhu, and Bo Zhang. Analytic-dpm: an analytic estimate of the optimal reverse variance in diffusion probabilistic models. In *International Conference on Learning Representations*, 2021.

Fan Bao, Chongxuan Li, Jiacheng Sun, Jun Zhu, and Bo Zhang. Estimating the optimal covariance with imperfect mean in diffusion probabilistic models. In *International Conference on Machine Learning*, pages 1555–1584. PMLR, 2022.

Soumya Basu, Branislav Kveton, Manzil Zaheer, and Csaba Szepesvári. No regrets for learning the prior in bandits. *Advances in Neural Information Processing Systems*, 34:28029–28041, 2021.

Tom Brown, Benjamin Mann, Nick Ryder, Melanie Subbiah, Jared D Kaplan, Prafulla Dhariwal, Arvind Neelakantan, Pranav Shyam, Girish Sastry, Amanda Askell, et al. Language models are few-shot learners. *Advances in neural information processing systems*, 33:1877–1901, 2020.

Sébastien Bubeck and Nicolò Cesa-Bianchi. Regret analysis of stochastic and nonstochastic multi-armed bandit problems. *Foundations and Trends in Machine Learning*, 5(1):1–122, 2012.

Leonardo Cella, Alessandro Lazaric, and Massimiliano Pontil. Meta-learning with stochastic linear bandits. In *International Conference on Machine Learning*, pages 1360–1370. PMLR, 2020.

Olivier Chapelle and Lihong Li. An empirical evaluation of Thompson sampling. In *Advances in Neural Information Processing Systems 24*, pages 2249–2257, 2012.

Ting Chen, Ruixiang Zhang, and Geoffrey Hinton. Analog bits: Generating discrete data using diffusion models with self-conditioning. *arXiv preprint arXiv:2208.04202*, 2022.

Hyungjin Chung, Jeongsol Kim, Michael T Mccann, Marc L Klasky, and Jong Chul Ye. Diffusion posterior sampling for general noisy inverse problems. *arXiv preprint arXiv:2209.14687*, 2022a.

Hyungjin Chung, Byeongsu Sim, and Jong Chul Ye. Come-closer-diffuse-faster: Accelerating conditional diffusion models for inverse problems through stochastic contraction. In *Proceedings of the IEEE/CVF Conference on Computer Vision and Pattern Recognition*, pages 12413–12422, 2022b.

Tim Dockhorn, Arash Vahdat, and Karsten Kreis. GENIE: Higher-Order Denoising Diffusion Solvers. In *Advances in Neural Information Processing Systems*, 2022.

Vincent Dutordoir, Alan Saul, Zoubin Ghahramani, and Fergus Simpson. Neural diffusion processes. *arXiv preprint arXiv:2206.03992*, 2022.

Yonina C Eldar. Generalized SURE for exponential families: Applications to regularization. *IEEE Transactions on Signal Processing*, 57(2):471–481, 2008.

Gersende Fort and Eric Moulines. Convergence of the monte carlo expectation maximization for curved exponential families. *The Annals of Statistics*, 31(4):1220–1259, 2003.

Alexandros Graikos, Nikolay Malkin, Nebojsa Jojic, and Dimitris Samaras. Diffusion models as plug-and-play priors. *arXiv preprint arXiv:2206.09012*, 2022.

Samarth Gupta, Shreyas Chaudhari, Subhojyoti Mukherjee, Gauri Joshi, and Osman Yağan. A unified approach to translate classical bandit algorithms to the structured bandit setting. *IEEE Journal on Selected Areas in Information Theory*, 1(3):840–853, 2020.

Jonathan Ho, Ajay Jain, and Pieter Abbeel. Denoising diffusion probabilistic models. *Advances in Neural Information Processing Systems*, 33:6840–6851, 2020.

Joey Hong, Branislav Kveton, Manzil Zaheer, Yinlam Chow, Amr Ahmed, and Craig Boutilier. Latent bandits revisited. In *Advances in Neural Information Processing Systems 33*, 2020.

Joey Hong, Branislav Kveton, Sumeet Katariya, Manzil Zaheer, and Mohammad Ghavamzadeh. Deep hierarchy in bandits. In *Proceedings of the 39th International Conference on Machine Learning*, 2022a.

Joey Hong, Branislav Kveton, Manzil Zaheer, Mohammad Ghavamzadeh, and Craig Boutilier. Thompson sampling with a mixture prior. In *International Conference on Artificial Intelligence and Statistics*, pages 7565–7586. PMLR, 2022b.

Timothy Hospedales, Antreas Antoniou, Paul Micaelli, and Amos Storkey. Meta-learning in neural networks: A survey. *IEEE transactions on pattern analysis and machine intelligence*, 44(9):5149–5169, 2021.

Michael Janner, Yilun Du, Joshua B Tenenbaum, and Sergey Levine. Planning with diffusion for flexible behavior synthesis. In *International Conference on Machine Learning*, 2022.

Tero Karras, Miika Aittala, Timo Aila, and Samuli Laine. Elucidating the design space of diffusion-based generative models. *arXiv preprint arXiv:2206.00364*, 2022.

Bahjat Kawar, Gregory Vaksman, and Michael Elad. SNIPS: Solving noisy inverse problems stochastically. In *Advances in Neural Information Processing Systems*, volume 34, pages 21757–21769, 2021.

Bahjat Kawar, Michael Elad, Stefano Ermon, and Jiaming Song. Denoising diffusion restoration models. In *Advances in Neural Information Processing Systems*, 2022.

Zhifeng Kong, Wei Ping, Jiaji Huang, Kexin Zhao, and Bryan Catanzaro. Diffwave: A versatile diffusion model for audio synthesis. In *International Conference on Learning Representations*, 2020.

Branislav Kveton, Mikhail Konobeev, Manzil Zaheer, Chih-wei Hsu, Martin Mladenov, Craig Boutilier, and Csaba Szepesvari. Meta-thompson sampling. In *International Conference on Machine Learning*, pages 5884–5893. PMLR, 2021.

Tor Lattimore and Remi Munos. Bounded regret for finite-armed structured bandits. In *Advances in Neural Information Processing Systems 27*, pages 550–558, 2014.

Tor Lattimore and Csaba Szepesvári. *Bandit algorithms*. Cambridge University Press, 2020.

Hairen Liao, Lingxiao Peng, Zhenchuan Liu, and Xuehua Shen. ipinyou global rtb bidding algorithm competition dataset. In *Proceedings of the Eighth International Workshop on Data Mining for Online Advertising*, pages 1–6, 2014.

Xiuyuan Lu and Benjamin Van Roy. Information-theoretic confidence bounds for reinforcement learning. In *Advances in Neural Information Processing Systems 32*, 2019.

Odalric-Ambrym Maillard and Shie Mannor. Latent bandits. In *Proceedings of the 31st International Conference on Machine Learning*, pages 136–144, 2014.

Christopher A Metzler, Ali Mousavi, Reinhard Heckel, and Richard G Baraniuk. Unsupervised learning with Stein's unbiased risk estimator. *arXiv preprint arXiv:1805.10531*, 2018.

Elvis Nava, Seijin Kobayashi, Yifei Yin, Robert K Katzschmann, and Benjamin F Grewe. Meta-learning via classifier (-free) guidance. *arXiv preprint arXiv:2210.08942*, 2022.

George Papandreou and Alan L Yuille. Gaussian sampling by local perturbations. *Advances in Neural Information Processing Systems*, 23, 2010.

Amit Peleg, Naama Pearl, and Ron Meir. Metalearning linear bandits by prior update. In *International Conference on Artificial Intelligence and Statistics*, pages 2885–2926. PMLR, 2022.

Sathish Ramani, Thierry Blu, and Michael Unser. Monte-Carlo SURE: A black-box optimization of regularization parameters for general denoising algorithms. *IEEE Transactions on image processing*, 17(9): 1540–1554, 2008.

Kashif Rasul, Calvin Seward, Ingmar Schuster, and Roland Vollgraf. Autoregressive denoising diffusion models for multivariate probabilistic time series forecasting. In *International Conference on Machine Learning*, pages 8857–8868. PMLR, 2021.

Jonas Rothfuss, Dominique Heyn, Andreas Krause, et al. Meta-learning reliable priors in the function space. *Advances in Neural Information Processing Systems*, 34:280–293, 2021.

Daniel Russo and Benjamin Van Roy. Learning to optimize via posterior sampling. *Mathematics of Operations Research*, 39(4):1221–1243, 2014.

Daniel J Russo, Benjamin Van Roy, Abbas Kazerouni, Ian Osband, Zheng Wen, et al. A tutorial on thompson sampling. *Foundations and Trends® in Machine Learning*, 11(1):1–96, 2018.

Chitwan Saharia, William Chan, Saurabh Saxena, Lala Li, Jay Whang, Emily Denton, Seyed Kamyar Seyed Ghasemipour, Burcu Karagol Ayan, S Sara Mahdavi, Rapha Gontijo Lopes, et al. Photorealistic text-to-image diffusion models with deep language understanding. *arXiv preprint arXiv:2205.11487*, 2022.

Tim Salimans and Jonathan Ho. Progressive distillation for fast sampling of diffusion models. In *International Conference on Learning Representations*, 2021.

Rajat Sen, Alexander Rakhlin, Lexing Ying, Rahul Kidambi, Dean Foster, Daniel Hill, and Inderjit Dhillon. Top-k extreme contextual bandits with arm hierarchy. In *Proceedings of the 38th International Conference on Machine Learning*, 2021.

Max Simchowitz, Christopher Tosh, Akshay Krishnamurthy, Daniel J Hsu, Thodoris Lykouris, Miro Dudik, and Robert E Schapire. Bayesian decision-making under misspecified priors with applications to meta-learning. *Advances in Neural Information Processing Systems*, 34:26382–26394, 2021.

Jascha Sohl-Dickstein, Eric Weiss, Niru Maheswaranathan, and Surya Ganguli. Deep unsupervised learning using nonequilibrium thermodynamics. In *International Conference on Machine Learning*, pages 2256–2265. PMLR, 2015.

Yang Song and Stefano Ermon. Generative modeling by estimating gradients of the data distribution. *Advances in Neural Information Processing Systems*, 32, 2019.

Yang Song, Jascha Sohfl-Dickstein, Diederik P Kingma, Abhishek Kumar, Stefano Ermon, and Ben Poole. Score-based generative modeling through stochastic differential equations. In *International Conference on Learning Representations*, 2020.

Yang Song, Liyue Shen, Lei Xing, and Stefano Ermon. Solving inverse problems in medical imaging with score-based generative models. In *International Conference on Learning Representations*, 2021.

Charles M Stein. Estimation of the mean of a multivariate normal distribution. *The annals of Statistics*, pages 1135–1151, 1981.

William R Thompson. On the likelihood that one unknown probability exceeds another in view of the evidence of two samples. *Biometrika*, 25(3-4):285–294, 1933.

Michal Valko, Remi Munos, Branislav Kveton, and Tomas Kocak. Spectral bandits for smooth graph functions. In *Proceedings of the 31st International Conference on Machine Learning*, pages 46–54, 2014.

Zachary Wu, Kadina E Johnston, Frances H Arnold, and Kevin K Yang. Protein sequence design with deep generative models. *Current opinion in chemical biology*, 65:18–27, 2021.

Han Xiao, Kashif Rasul, and Roland Vollgraf. Fashion-mnist: a novel image dataset for benchmarking machine learning algorithms. *arXiv preprint arXiv:1708.07747*, 2017.

Hongkai Zheng, Weili Nie, Arash Vahdat, Kamyar Azizzadenesheli, and Anima Anandkumar. Fast sampling of diffusion models via operator learning. *arXiv preprint arXiv:2211.13449*, 2022.

Magauiya Zhussip, Shakarim Soltanayev, and Se Young Chun. Extending stein's unbiased risk estimator to train deep denoisers with correlated pairs of noisy images. *Advances in neural information processing systems*, 32, 2019.

Appendix

A Mathematics of Algorithm Design

In this appendix we provide mathematical derivations that inspire the design of several components of our algorithms.

A.1 Recurrent Step in Posterior Sampling from Diffusion Prior

We provide below the derivation of the recurrent step of our posterior sampling algorithm (Algorithm 3) that samples from $X_L \,|\, x_{\ell+1}, y_0$. For this, we write

$$q(x_\ell \,|\, x_{\ell+1}, y_0) = \frac{q(x_\ell \,|\, x_{\ell+1}) q(y_0 \,|\, x_\ell, x_{\ell+1})}{q(y_0 \,|\, x_{\ell+1})} = \frac{q(x_\ell \,|\, x_{\ell+1}) \int q(y_0 \,|\, x_0) q(x_0 \,|\, x_\ell, x_{\ell+1}) \, dx_0}{q(y_0 \,|\, x_{\ell+1})}. \tag{9}$$

The term $q(x_\ell \,|\, x_{\ell+1})$ can be simply approximated with $p_{\theta,\tau}(x_\ell \,|\, x_{\ell+1})$. As for the integral, one natural solution is to use $q(x_0 \,|\, x_\ell, x_{\ell+1}) = q(x_0 \,|\, x_\ell) \approx p'_{\theta,\tau}(x_0 \,|\, x_\ell)$. Then, for example, if $q(y_0 \,|\, x_0) = \mathcal{N}(y_0; x_0, \sigma^2 I)$, we can deduce

$$\int q(y_0 \,|\, x_0) p'_\theta(x_0 \,|\, x_\ell) \, dx_0 = \mathcal{N}(y_0; h_\theta(x_\ell, \ell), \sigma^2 I + \operatorname{diag}(\tau_\ell^2)).$$

Nonetheless, as the denoiser h_θ can be arbitrarily complex, this does not lead to a close form expression to sample x_ℓ. Therefore, to avoid the use of involved sampling strategy in the recurrent step, we approximate $q(x_0 \,|\, x_\ell, x_{\ell+1})$ in a different way. We first recall that by definition of the diffusion model we may write

$$X_\ell = \sqrt{\bar\alpha_\ell} X_0 + \sqrt{1 - \bar\alpha_\ell} \bar Z_\ell \quad \text{and} \quad X_{\ell+1} = \sqrt{\alpha_{\ell+1}} X_\ell + \sqrt{1 - \alpha_\ell} Z_{\ell+1},$$

where both $\bar Z_\ell$ and $Z_{\ell+1}$ are random variable with distribution $\mathcal{N}(0, I)$. This leads to

$$X_{\ell+1} = \sqrt{\bar\alpha_{\ell+1}} X_0 + \sqrt{1 - \bar\alpha_{\ell+1}} \bar Z_{\ell+1}$$

where

$$\bar Z_{\ell+1} = \sqrt{\frac{\alpha_{\ell+1}(1 - \bar\alpha_\ell)}{1 - \bar\alpha_{\ell+1}}} \bar Z_\ell + \sqrt{\frac{1 - \alpha_{\ell+1}}{1 - \bar\alpha_{\ell+1}}} Z_{\ell+1}.$$

Therefore, we may take $\bar Z_{\ell+1}$ as a reasonable approximation of $\bar Z_\ell$, while sampling $\bar Z_{\ell+1}$ is basically the same as sampling from $p'_\theta(X_0 \,|\, x_{\ell+1})$. To summarize, we write

$$\begin{aligned}
q(x_0 \,|\, x_\ell, x_{\ell+1}) &= q\left(\bar Z_\ell = \frac{x_\ell - \sqrt{\bar\alpha_\ell} x_0}{\sqrt{1 - \bar\alpha_\ell}} \,\middle|\, x_\ell, x_{\ell+1} \right) \\
&\approx q\left(\bar Z_{\ell+1} = \frac{x_\ell - \sqrt{\bar\alpha_\ell} x_0}{\sqrt{1 - \bar\alpha_\ell}} \,\middle|\, x_\ell, x_{\ell+1} \right) \\
&= q\left(X_0 = \frac{1}{\sqrt{\bar\alpha_{\ell+1}}} \left(x_{\ell+1} - (x_\ell - \sqrt{\bar\alpha_\ell} x_0) \sqrt{\frac{1 - \bar\alpha_{\ell+1}}{1 - \bar\alpha_\ell}} \right) \,\middle|\, x_\ell, x_{\ell+1} \right) \\
&\approx p'_{\theta,\tau}\left(X_0 = \frac{1}{\sqrt{\bar\alpha_{\ell+1}}} \left(x_{\ell+1} - (x_\ell - \sqrt{\bar\alpha_\ell} x_0) \sqrt{\frac{1 - \bar\alpha_{\ell+1}}{1 - \bar\alpha_\ell}} \right) \,\middle|\, x_{\ell+1} \right) \\
&= \mathcal{N}\left(\sqrt{\frac{\bar\alpha_\ell (1 - \bar\alpha_{\ell+1})}{\bar\alpha_{\ell+1}(1 - \bar\alpha_\ell)}} x_0 + \frac{x_{\ell+1}}{\sqrt{\bar\alpha_{\ell+1}}} - \sqrt{\frac{1 - \bar\alpha_{\ell+1}}{\bar\alpha_{\ell+1}(1 - \bar\alpha_\ell)}} x_\ell \,;
\end{aligned}$$

$$h_\theta(x_{\ell+1}, \ell+1), \operatorname{diag}(\tau^2_{\ell+1})\Big)$$
$$= \sqrt{\rho_\ell}\,\mathcal{N}\left(x_0\,;\, \frac{1}{\sqrt{\bar\alpha_\ell}}(x_\ell - \sqrt{1-\bar\alpha_\ell}\,\bar z_{\ell+1}), \rho_\ell \operatorname{diag}(\tau^2_{\ell+1})\right),$$

where $\rho_\ell = \bar\alpha_{\ell+1}(1-\bar\alpha_\ell)/(\bar\alpha_\ell(1-\bar\alpha_{\ell+1}))$ and $\bar z_{\ell+1}$ represents the noise predicted by the denoiser from $x_{\ell+1}$, that is,

$$\bar z_{\ell+1} = \frac{x_{\ell+1} - \sqrt{\bar\alpha_{\ell+1}}h_\theta(x_{\ell+1}, \ell+1)}{\sqrt{1-\bar\alpha_{\ell+1}}}.$$

In this way, we have approximated $q(x_0 \,|\, x_\ell, x_{\ell+1})$ by a Gaussian with diagonal covariance and with mean that depends only linearly on x_ℓ. In the multi-armed bandit setup that we consider here, the relation between y_0 the interaction history and $x_0 = \mu$ the mean reward vector obeys (3). There exists thus $C(y_0)$ and $\widetilde C(y_0)$ such that

$$\underbrace{\int q(y_0 \,|\, x_0) q(x_0 \,|\, x_\ell, x_{\ell+1})\, dx_0}_{A} = \int C(y_0) \prod_{s=1}^{t} \mathcal{N}(r_s; \mu^{a_s}, \sigma^2) q(x_0 \,|\, x_\ell, x_{\ell+1})\, dx_0$$
$$= \int \widetilde C(y_0) \prod_{\substack{a\in\mathcal{A}\\ N_t^a>0}} \mathcal{N}(\hat\mu_t^a; \mu^a, (\sigma_t^a)^2) q(x_0 \,|\, x_\ell, x_{\ell+1})\, dx_0.$$

Using $x_0 = \mu$, the aforementioned approximation of $q(x_0 \,|\, x_\ell, x_{\ell+1})$, and ignoring the multiplicative constant that does not depend on x_ℓ, we get

$$\begin{aligned}
A &\propto \int \prod_{\substack{a\in\mathcal{A}\\ N_t^a>0}} \mathcal{N}(\hat\mu_t^a; x_0^a, (\sigma_t^a)^2) q(x_0 \,|\, x_\ell, x_{\ell+1})\, dx_0 \\
&\approx \sqrt{\rho_\ell} \int \prod_{\substack{a\in\mathcal{A}\\ N_t^a>0}} \mathcal{N}(\hat\mu_t^a; x_0^a, (\sigma_t^a)^2) \prod_{a\in\mathcal{A}} \mathcal{N}\left(x_0^a; \frac{1}{\sqrt{\bar\alpha_\ell}}(x_\ell^a - \sqrt{1-\bar\alpha_\ell}\,\bar z_{\ell+1}^a), \rho_\ell(\tau_{\ell+1}^a)^2\right) dx_0 \\
&= \sqrt{\rho_\ell} \prod_{\substack{a\in\mathcal{A}\\ N_t^a>0}} \int \mathcal{N}(\hat\mu_t^a; x_0^a, (\sigma_t^a)^2) \mathcal{N}\left(x_0^a; \frac{1}{\sqrt{\bar\alpha_\ell}}(x_\ell^a - \sqrt{1-\bar\alpha_\ell}\,\bar z_{\ell+1}^a), \rho_\ell(\tau_{\ell+1}^a)^2\right) dx_0^a \\
&= \sqrt{\rho_\ell} \prod_{\substack{a\in\mathcal{A}\\ N_t^a>0}} \mathcal{N}\left(\hat\mu_t^a; \frac{1}{\sqrt{\bar\alpha_\ell}}(x_\ell^a - \sqrt{1-\bar\alpha_\ell}\,\bar z_{\ell+1}^a), (\sigma_t^a)^2 + \rho_\ell(\tau_{\ell+1}^a)^2\right) \\
&\propto \prod_{\substack{a\in\mathcal{A}\\ N_t^a>0}} \mathcal{N}\left(x_\ell^a; \sqrt{\bar\alpha_\ell}\hat\mu_t^a + \sqrt{1-\bar\alpha_\ell}\,\bar z_{\ell+1}^a, \bar\alpha_\ell((\sigma_t^a)^2 + \rho_\ell(\tau_{\ell+1}^a)^2).\right)
\end{aligned}$$

Plugging the above into (9), we obtain $\tilde q(x_\ell \,|\, x_{\ell+1}, y_0) = \prod_{a\in\mathcal{A}} \tilde q(x_\ell^a \,|\, x_{\ell+1}, y_0)$ where $\tilde q(x_\ell^a \,|\, x_{\ell+1}, y_0) = p_{\theta,\tau}(x_\ell^a \,|\, x_{\ell+1})$ if a is never pulled and otherwise it is the distribution satisfying

$$\tilde q(x_\ell^a \,|\, x_{\ell+1}, y_0) \propto p_{\theta,\tau}(x_\ell^a \,|\, x_{\ell+1}) \mathcal{N}\left(x_\ell^a; \sqrt{\bar\alpha_\ell}\hat\mu_t^a + \sqrt{1-\bar\alpha_\ell}\,\bar z_{\ell+1}^a, \bar\alpha_\ell((\sigma_t^a)^2 + \rho_\ell(\tau_{\ell+1}^a)^2)\right). \tag{10}$$

To conclude, we resort to the following lemma (see [Papandreou and Yuille, 2010] for more general results).

Lemma 1. *Let $\mu_1, \mu_2, \sigma_1, \sigma_2 \in \mathbb{R}$. The following two sampling algorithms are equivalent.*

1. *Sample x directly from the distribution whose density is proportional the product $\mathcal{N}(\mu_1, \sigma_1^2)\mathcal{N}(\mu_2, \sigma_2^2)$.*
2. *Sample x_1 from $\mathcal{N}(\mu_1, \sigma_1^2)$, x_2 from $\mathcal{N}(\mu_2, \sigma_2^2)$, and compute $x = \sigma_1^{-2}x_1 + \sigma_2^{-2}x_2/(\sigma_1^{-2} + \sigma_2^{-2})$.*

Proof. It is well known that the product of two Gaussian PDFs is itself proportional to a Gaussian PDF. Concretely, we have

$$\mathcal{N}(\mu_1, \sigma_1^2)\mathcal{N}(\mu_2, \sigma_2^2) \propto \mathcal{N}\left(\frac{\sigma_1^{-2}\mu_1 + \sigma_2^{-2}\mu_2}{\sigma_1^{-2} + \sigma_2^{-2}}, \frac{1}{\sigma_1^{-2} + \sigma_2^{-2}}\right). \tag{11}$$

On the other hand, the linear combination of two independent Gaussian variables is also a Gaussian variable. For X_1, X_2 that follow $\mathcal{N}(\mu_1, \sigma_1^2), \mathcal{N}(\mu_2, \sigma_2^2)$ and $X = \sigma_1^{-2}X_1 + \sigma_2^{-2}X_2/(\sigma_1^{-2} + \sigma_2^{-2})$, we can compute

$$\mathbb{E}[X] = \frac{\sigma_1^{-2}\,\mathbb{E}[X_1] + \sigma_2^{-2}\,\mathbb{E}[X_2]}{\sigma_1^{-2} + \sigma_2^{-2}} = \frac{\sigma_1^{-2}\mu_1 + \sigma_2^{-2}\mu_2}{\sigma_1^{-2} + \sigma_2^{-2}},$$

$$\mathrm{Var}[X] = \frac{\sigma_1^{-4}\,\mathrm{Var}[X_1] + \sigma_2^{-4}\,\mathrm{Var}[X_2]}{(\sigma_1^{-2} + \sigma_2^{-2})^2} = \frac{\sigma_1^{-2} + \sigma_2^{-2}}{(\sigma_1^{-2} + \sigma_2^{-2})^2} = \frac{1}{\sigma_1^{-2} + \sigma_2^{-2}}.$$

Therefore, X follows the distribution of (11) and computing the linear combination of x_1 and x_2 as suggested is equivalent to sampling directly from the resulting distribution. □

We obtain the algorithm presented in Section 3.2 by applying Lemma 1 to (10) with

$$\mathcal{N}(\mu_1, \sigma_1^2) \leftarrow p_{\theta,\tau}(x_\ell^a \mid x_{\ell+1})$$
$$\mathcal{N}(\mu_2, \sigma_2^2) \leftarrow \mathcal{N}\left(x_\ell^a; \sqrt{\bar{\alpha}_\ell}\hat{\mu}_t^a + \sqrt{1-\bar{\alpha}_\ell}\bar{z}_{\ell+1}^a, \bar{\alpha}_\ell((\sigma_t^a)^2 + \rho_\ell(\tau_{\ell+1}^a)^2)\right).$$

A.2 On SURE-based Regularization

In this part we show how the loss function (7) is related to Stein's unbiased risk estimate (SURE). We first note that by definition of the diffusion process, we have $x_\ell = \sqrt{\bar{\alpha}_\ell}x_0 + \sqrt{1-\bar{\alpha}_\ell}\bar{z}_\ell$ where $\bar{z}_\ell$ is a random variable following the distribution $\mathcal{N}(0,1)$. Moreover, $\sqrt{\bar{\alpha}_\ell}h_\theta(x_\ell, \ell)$ is an estimator of $\sqrt{\bar{\alpha}_\ell}x_0$ from x_ℓ. The corresponding SURE thus writes

$$\mathrm{SURE}(\sqrt{\bar{\alpha}_\ell}h_\theta(\cdot, \ell)) = \|\sqrt{\bar{\alpha}_\ell}h_\theta(x_\ell, \ell) - x_\ell\|^2 - K(1-\bar{\alpha}_\ell) + 2(1-\bar{\alpha}_\ell)\,\mathrm{div}_{x_\ell}(\sqrt{\bar{\alpha}_\ell}h_\theta(x_\ell, \ell)).$$

If it holds $x_\ell = \sqrt{\bar{\alpha}_\ell}y_0$ while y_0 follows the distribution $\mathcal{N}(x_0, \sigma^2 I)$, we get immediately $1 - \bar{\alpha}_\ell = \bar{\alpha}_\ell\sigma^2$. The above can thus be rewritten as

$$\mathrm{SURE}(\sqrt{\bar{\alpha}_\ell}h_\theta(\cdot, \ell)) = \|\sqrt{\bar{\alpha}_\ell}h_\theta(x_\ell, \ell) - \sqrt{\bar{\alpha}_\ell}y_0\|^2 - K\bar{\alpha}_\ell\sigma^2 + 2\bar{\alpha}_\ell^{\frac{3}{2}}\sigma^2\,\mathrm{div}_{x_\ell}(h_\theta(x_\ell, \ell)).$$

Dividing the above by $\bar{\alpha}_\ell$ we get an unbiased estimate of $\mathbb{E}[\|h_\theta(x_\ell, \ell) - x_0\|^2]$, i.e.,

$$\mathbb{E}[\|h_\theta(x_\ell, \ell) - x_0\|^2] = \mathbb{E}[\|h_\theta(x_\ell, \ell) - y_0\|^2 - K\sigma^2 + 2\sqrt{\bar{\alpha}_\ell}\sigma^2\,\mathrm{div}_{x_\ell}(h_\theta(x_\ell, \ell))].$$

On the right hand side inside expectation we recover Eq. (7) with $m = \mathbf{1}$ and $\lambda = 1$ by replacing x_ℓ by $\tilde{x}_\ell$ and the divergence by its Monte-Carlo approximation [Ramani et al., 2008].

B Missing Experimental Details

In this section, we provide missing experimental details mainly concerning the construction of the problem instances and the learning of priors. All the simulations are run on an Amazon p3.2xlarge instance equipped with 8 NVIDIA Tesla V100 GPUs.

B.1 Construction of Bandit Instances

We provide below more details on how the bandit instances are constructed in our problems. Besides the three problems described in Section 5, we consider an additional `Labeled Arms` problem that will be used for our ablation study. Some illustrations of the constructed instances and the vectors generated by learned priors are provided in Appendix E. As in `Popular and Niche` and `2D Maze` problems, in the `Labeled Arms` problem we simply add Gaussian noise of standard deviation 0.1 to the mean when sampling the reward. For these three problems we thus only explain how the means are constructed.

1. `Popular and Niche` ($K = 200$ arms). The arms are split into 40 groups of equal size. 20 of these groups represent the 'popular' items while the other 20 represent the 'niche' items. For each bandit task, we first construct a vector $\bar{\mu}$ whose coordinates' values default to 0. However, we randomly choose 1 to 3 groups of niche items and set the value of each of these items to 1 with probability 0.7 (independently across the selected items). Similarly, we randomly choose 15 to 17 groups of popular items and set their values to 0.8. Then, to construct the mean reward vector μ, we perturb the values of $\bar{\mu}$ by independent Gaussian noises with standard deviation of 0.1. After that, we clip the values of the popular items to make them smaller than 0.95 and clip the entire vector to the range $[0, 1]$.

2. `iPinYou bidding` ($K = 300$ arms). The set of tasks is constructed with the help of the iPinYou data set [Liao et al., 2014]. This data set contains logs of ad biddings, impressions, clicks, and final conversions, and is separated into three different seasons. We only use the second season that contains the ads from 5 advertisers (as we are not able to find the data for the first and the third season). To form the tasks, we further group the bids according to the associated ad slots. By keeping only those ad slots with at least 1000 bids, we obtain a data set of 1352 ad slots. Then, the empirical distribution of the paying price (i.e., the highest bid from competitors) of each ad slot is used to computed the success rate of every potential bid $b \in \{0, \dots, 299\}$ set by the learner. The reward is either $300 - b$ when the learner wins the auction or 0 otherwise. Finally, we divide everything by the largest reward that the learner can ever get in all the tasks to scale the rewards to range $[0, 1]$.

3. `2D Maze` ($K = 180$ base arms). For this problem, we first use the code of the github repository `MattChanTK/gym-maze`[10] to generate random 2D mazes of size 19×19. Then, each bandit task can be derived from a generated 2D maze by associating the maze to a weighted 10×10 grid graph. As demonstrated by Figure 4, each case corresponds to either a node or an edge of the grid graph. Then, the weight (mean reward) of an edge (base arms) is either -1 or -0.01 depending on either there is a wall (in black color) or not (in white color) on the corresponding case. An optimal arm in this problem would be a path that goes from the source to the destination without bumping into any walls in the corresponding maze.

4. `Labeled Arms` ($K = 500$ arms). This problem is again inspired by applications in recommendation systems. We are provided here a set of 50 labels $\mathcal{L} = \{1, ..., 50\}$. Each arm is associated to a subset $\mathcal{L}^a$ of these labels with size $\text{card}(\mathcal{L}^a) = 7$. To sample a new bandit task B, we randomly draw a set $\mathcal{L}_B \subseteq \mathcal{L}$ again with size 7. Then for each arm a, we set $\bar{\mu}^a = 1 - 1/4^{\text{card}(\mathcal{L}^a \cap \mathcal{L}_B)}$ so that the more the two sets intersect the higher the value. Finally, to obtain the mean rewards μ, we perturb the coordinates of $\bar{\mu}$ by independent Gaussian noises of standard deviation 0.1 and scale the resulting vector to the range $[0, 1]$.

Training, Calibration, and Test Sets. Training, calibration, and test set are constructed for each of the considered problem. Their size are fixed at 5000, 1000, 100 for the `Popular and Niche`, `2D Maze`, and `Labeled Arms` Problems, and at 1200, 100, and 52 for the `iPinYou Bidding` problem.

B.2 Diffusion Models– Model Design

In all our experiments (including the ones described in Appendices C and D), we set the diffusion steps of the diffusion models to $L = 100$ and adopt a linear variance schedule that varies from $1 - \alpha_1 = 10^{-4}$ to $1 - \alpha_L = 0.1$. The remaining details are customized to each problem, taking into account the specificity of the underlying data distribution.

1. `Labeled Arms` and `Popular and Niche`. These two problems have the following two important features: (*i*) The expected means of the bandit instances do not exhibit any spatial correlations (see Figures 16a and 17a). (*ii*) The values of the expected means are nearly binary.

[10] https://github.com/MattChanTK/gym-maze

The first point prevents us from using the standard U-Net architecture. Instead, we consider an architecture adapted from Kong et al. [2020], Rasul et al. [2021], with 5 residual blocks and each block containing 6 residual channels.[11] Then, to account for the lack of spatial correlations, we add a fully connected layer at the beginning to map the input to a vector of size 128×6, before reshaping these vectors into 6 channels and feeding them to the convolutional layers. In a similar fashion, we also replace the last layer of the architecture by a fully connected layer that maps a vector of size 128×6 to a vector of size K. We find that these minimal modification already enable the model to perform well on these two problems.

As for the latter point, we follow Chen et al. [2022] and train the denoisers to predict the clean sample x_0 as it is reported in the said paper that this leads to better performance when the data are binary.

2. `iPinYou Bidding`. As shown in Figure 20, the pattern of this problem looks similar to that of natural images. We therefore adopt the standard U-Net architecture, with an adaption to the 1-dimensional case as described by [Janner et al., 2022]. The model has three feature map resolutions (from 300 to 75) and the number of channels for each resolution is respectively 16, 32, and 64. No attention layer is used. The denoiser is trained to predict noise as in Ho et al. [2020], Song and Ermon [2019].

3. `2D Maze` As explained in Appendix B.1 and illustrated in Figure 4, the weighted grid graphs are themselves derived by the 2D mazes. We can accordingly establish a function that maps each 10×10 weighted grid graph to an image of size 19×19 and vice-versa— it suffices to match the value of each associated (edge, pixel) pair. For technical reason, we further pad the 19×19 images to size 20×20 by adding one line of -1 at the right and one row of -1 at the bottom (see Figure 21). We then train diffusion models to learn the distribution of the resulting images. For this, we use a 2-dimensional U-Net directly adapted from the ones used by Ho et al. [2020]. The model has three feature map resolutions (from 20×20 to 5×5) and the number of channels for each resolution is respectively 32, 64, and 128. A self-attention block is used at every resolution. We again train the denoiser to predict the clean sample x_0 as we have binary expected rewards here (-0.01 or -1).

B.3 Diffusion Models– Training

Through out our experiments, we use Adam optimizer with learning rate 5×10^{-4} and exponential decay rates $\beta_1 = 0.9$ and $\beta_2 = 0.99$. The batch size and the epsilon constant in SURE-based regularization are respectively fixed at 128 and $\epsilon = 10^{-5}$. When the perfect data sets $\mathcal{D}_{\text{tr}}$ and $\mathcal{D}_{\text{cal}}$ are provided, we simply train the diffusion models for 15000 steps on the training set $\mathcal{D}_{\text{tr}}$ and apply Algorithm 2 on the calibration set $\mathcal{D}_{\text{cal}}$ to calibrate the variances. The training procedure is more complex when only imperfect data are available. We provide the details below.

Posterior Sampling. As explained in Section 4 and Algorithm 5, to train from imperfect data we sample the entire chain of diffused samples $\tilde{x}_{0:L}$ from the posterior. However, while Algorithm 3 performs sampling with predicted noise $\bar{z}_{\ell+1}$ and as we will show in Appendix D.2, this indeed leads to improved performance in a certain aspect, we observe that when used for training, it prevents the model from making further progress. We believe this is because in so doing we are only reinforcing the current model with their own predictions. Therefore, to make the method effective, in our experiments we slightly modify the posterior sampling algorithm that is used during training. While we still construct samples $x_{0:L}$ following Algorithm 3, the samples $\tilde{x}_{0:L}$ used for the loss minimization phase are obtained by replacing $\bar{z}_{\ell+1}$ (line 9) by $\tilde{z}_{\ell+1}$ sampled from $\mathcal{N}(0, I)$ in the very last sampling step. That is, from $x_{\ell+1}$ we sample both x_ℓ for further iterations of the algorithm and $\tilde{x}_\ell$ to be used for loss minimization.

Training Procedure Specification. When training and validation data are incomplete and noisy, we follow the training procedure described in Algorithm 5 with default values $S = 15000$ warm-up steps, $J = 3$ repeats, and $S' = 3000$ steps within each repeat (thus 24000 steps in total). Moreover, during the warm-up phase we impute the missing value with constant 0.5 when constructing the diffused samples $\tilde{x}_\ell$. As for

[11] These numbers are rather arbitrary and do not seem to affect much our results.

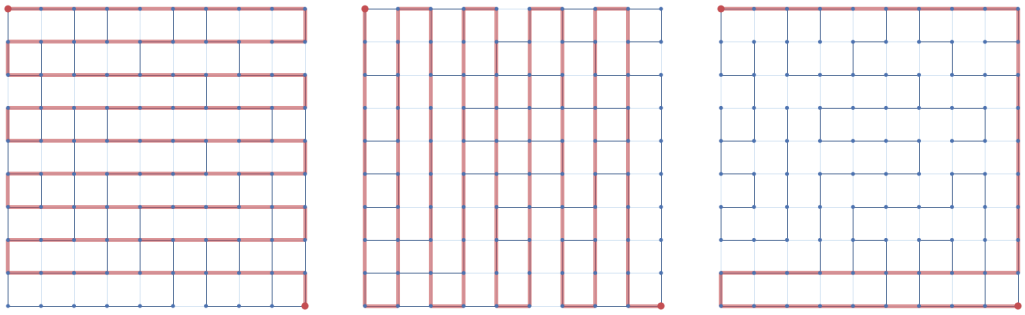

Figure 6: The three paths (super-arms) for UCB initialization in the `2D Maze` experiment.

the regularization parameter λ, we fix it at 0.1 for the `Popular and Niche`, `2D Maze`, and `Labeled Arms` problems.

Nevertheless, training from imperfect data turns out to be difficult for the iPinYou Bidding problem. We conjecture this is both because the training set is small and because we train the denoiser to predict noise here. Two modifications are then brought to the above procedure to address the additional difficulty. First, as SURE-based regularization can prevent the model from learning any pattern from data when information is scarce, we drop it for the warm-up phase and the first two repeats (i.e., the first 21000 steps). We then get a model that has learned the noisy distribution. We then add back SURE-based regularization with $\lambda = 0.25$ in the third repeat. After the 24000 steps, the model is good enough at reconstructing the corrupted data set, but the unconditionally generated samples suffer from severe mode collapse. Provided that the reconstructed samples are already of good quality, we fix the latter issue simply by applying standard training on the reconstructed samples for another 3000 steps (thus 27000 training steps in total).

B.4 Other Details

In this part we provide further details about the evaluation phase and the baselines.

Assumed Noise Level. All the bandit algorithms considered in our work take as input a hyperparameter $\hat{\sigma}$ that should roughly be in the order of the scale of the noise. For the results presented in Section 5, we set $\hat{\sigma} = 0.1$ for the `Popular and Niche` and `2D Maze` problems and $\hat{\sigma} = 0.2$ for the `iPinYou Bidding` problem. The former is exactly the ground truth standard deviation of the underlying noise distribution. For the `iPinYou Bidding` problem the noise is however not Gaussian, and $\hat{\sigma} = 0.2$ is approximately the third quartile of the empirical distribution of the expected rewards' standard deviations (computed across tasks and arms). In Appendix D.1, we present additional results for algorithms run with different assumed noise levels $\hat{\sigma}$.

UCB. The most standard implementation of the UCB algorithm sets the upper confidence bound to

$$U_t^a = \hat{\mu}_t^a + \hat{\sigma}\sqrt{\frac{2\log t}{N_t^a}}. \tag{12}$$

Instead, in our experiments we use $U_t^a = \hat{\mu}_t^a + \hat{\sigma}/\sqrt{N_t^a}$. Eq. (12) is more conservative than our implementation, and we thus do not expect it to yield smaller regret within the time horizon of our experiments.

UCB Initialization. In contrary to Thompson sampling-based methods, UCB typically requires an initialization phase. For vanilla multi-armed bandits (`Popular and Niche`, `iPinYou Bidding`, and `Labeled Arms`) this simply consists in pulling each arm once. For combinatorial bandits we need to pull a set of super arms that covers all the base arms. In the `2D Maze` experiment we choose the three paths shown in Figure 6.

Gaussian Prior with Imperfect Data. To fit a Gaussian on incomplete and noisy data, we proceed as follows: First, we compute the mean of arm a from those samples that have observation for a. Next, in a similar fashion, the covariance between any two arms are only computed with samples that have observations for both arms. Let the resulting matrix be $\hat{\Sigma}$. Since the covariance matrix of the sum of two independently distributed random vectors (in our case X_0 and noise) is the sum of the covariance matrices of the two random vectors, we further compute $\hat{\Sigma}' = \hat{\Sigma} - \sigma^2 I$ as an estimate of the covariance matrix of X_0. Finally, as $\hat{\Sigma}'$ is not necessarily positive semi-definite and can even have negative diagonal entries, for TS with diagonal covariance matrix we threshold the estimated variances to be at least 0 and for TS with full covariance matrix we threshold the eigenvalues of the estimated covariance matrix $\hat{\Sigma}'$ to be at least 10^{-4}.[12]

Arm Selection in `2D Maze` Problem. All the algorithms we use in the `2D Maze` problem first compute/sample some values for each base arm (edge) and then select the super arm (path) that maximizes the sum of its base arms' values (for DiffTS we first map the sampled 20×20 image back to a weighted graph and the remaining is the same). Concretely, we implement this via Dijkstra's shortest path algorithm applied to the weighted graphs with weights defined as the opposite of the computed/sampled values. However, these weights are not guaranteed to be non-negative, and we thus clip all the negative values to 0 before computing the shortest path.

C Ablation Study

In this appendix, we perform ablation studies on the `Popular and Niche` and `Labeled Arms` problems to explore the impacts of various design choices of our algorithms.

C.1 Predicted versus Sampled Noise in Posterior Sampling

In the DiffTS scheme that we develop (Algorithms 3 and 4), we propose to use the predicted noise $\bar{z}_{\ell+1}$ in the construction of the diffused observation $\tilde{y}_\ell$. Alternatively, we can replace it by the sampled noise vector $\tilde{z}_{\ell+1}$ (the resulting algorithm then becomes very similar to the one proposed in Song et al. [2021]). In Figure 9, we investigate how this decision affects the performance of DiffTS with diffusion priors trained on perfect data set $\mathcal{D}_{\text{tr}}$. It turns out that for the two problems considered here, there is not clear winner between the two options. However, it seems that using only sampled noise produces noisier samples, which leads to significant increase in regret in the `Labeled Arms` problem. We further confirm this intuition in Appendix D.2, where we show on a toy problem that the use of predicted noise often leads to samples that are more consistent with the learned prior. However, this does not always lead to performance improvement in bandit problems as the learned prior is never perfect.

C.2 Importance of Variance Calibration

Throughout our work, we have highlighted multiple times the importance of equipping the diffusion model with a suitable variance estimate. We demonstrate this in Figure 8. We consider diffusion priors trained on the perfect data set $\mathcal{D}_{\text{tr}}$ along with three different reverse variance schedules: (*i*) calibrated, i.e., Eq. (2); (*ii*) non-calibrated, i.e., Eq. (1); (*iii*) partially calibrated– precisely, only the variance of $X_0 \,|\, x_1$ is calibrated. We see clearly that a non-calibrated reverse variance schedule leads catastrophic regret performance. This is because the sampling process relies too much on the learned model; in particular, the variance of $p_\theta(X_0 \,|\, x_1)$ is fixed at zero. Instead, calibrating $X_0 \,|\, x_1$ itself already leads to significant decrease in regret, making it as competitive as (and sometimes even better than) the fully calibrated alternative. This suggests that the trade-off between the learned model and the observations mainly occurs at the last reverse step, whereas enlarging the variance of the remaining reverse steps has little to no effect. [Yet, it is also clear from the

[12] Our implementation requires the prior covariance matrix to be positive definite.

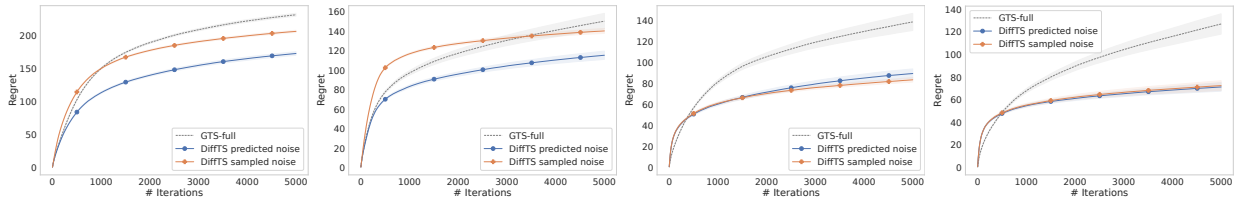

`Labeled Arms` $\hat{\sigma} = 0.1$ `Labeled Arms` $\hat{\sigma} = 0.05$ `Popular & Niche` $\hat{\sigma} = 0.1$ `Popular & Niche` $\hat{\sigma} = 0.05$

Figure 7: Regret comparison for DiffTS with predicted or independently sampled noise in the construction of diffused observation $\tilde{y}_\ell$.

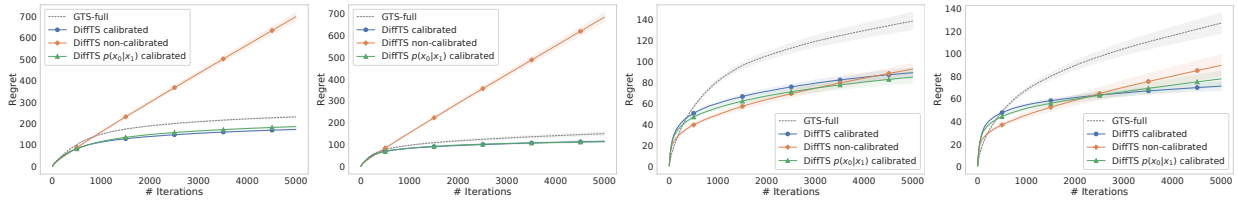

`Labeled Arms` $\hat{\sigma} = 0.1$ `Labeled Arms` $\hat{\sigma} = 0.05$ `Popular & Niche` $\hat{\sigma} = 0.1$ `Popular & Niche` $\hat{\sigma} = 0.05$

Figure 8: Regret comparison for DiffTS with three different types of reverse variance schedules.

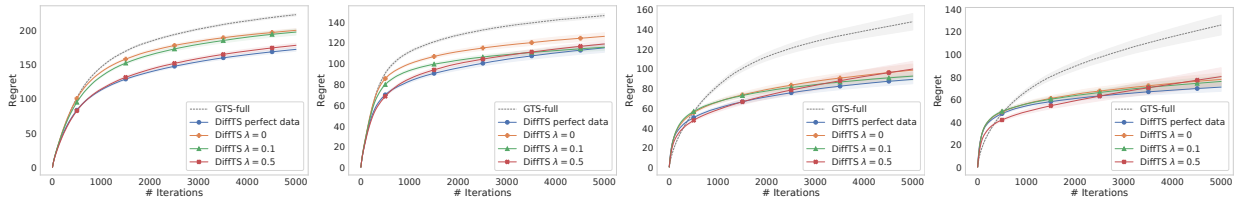

`Labeled Arms` $\hat{\sigma} = 0.1$ `Labeled Arms` $\hat{\sigma} = 0.05$ `Popular & Niche` $\hat{\sigma} = 0.1$ `Popular & Niche` $\hat{\sigma} = 0.05$

Figure 9: Regret comparison for DiffTS trained on noisy data with different regularization weight λ.

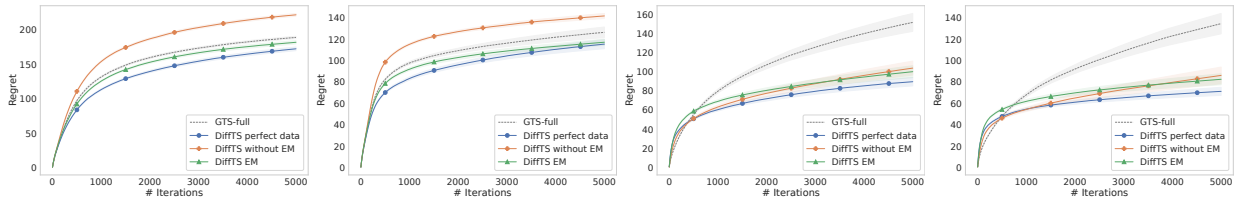

`Labeled Arms` $\hat{\sigma} = 0.1$ `Labeled Arms` $\hat{\sigma} = 0.05$ `Popular & Niche` $\hat{\sigma} = 0.1$ `Popular & Niche` $\hat{\sigma} = 0.05$

Figure 10: Regret comparison for DiffTS trained on incomplete data with or without EM.

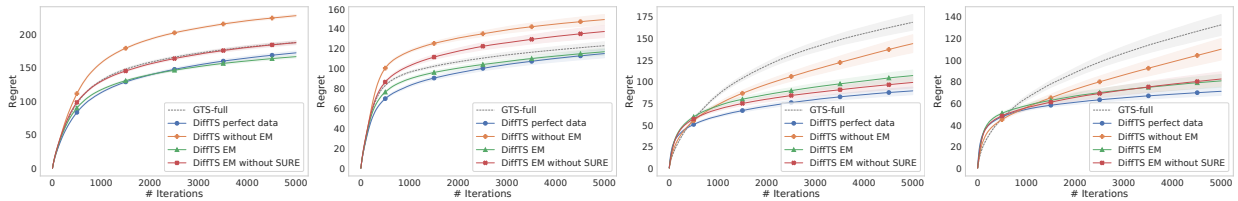

`Labeled Arms` $\hat{\sigma} = 0.1$ `Labeled Arms` $\hat{\sigma} = 0.05$ `Popular & Niche` $\hat{\sigma} = 0.1$ `Popular & Niche` $\hat{\sigma} = 0.05$

Figure 11: Regret comparison for DiffTS trained on noisy and incomplete data with or without EM / SURE-based regularization.

experiment on the `Popular and Niche` problem with presumed noise standard deviation 0.5 that calibrating the variance of all the reverse steps may still be beneficial in some situation.]

C.3 Ablation Study for Training from Imperfect Data

Our algorithm for training from imperfect data (Algorithm 5) makes two important modifications to the original training scheme: the Expectation Maximization-like procedure (abbreviated as EM hereinafter) and the use of SURE-based regularization. Below we discuss their effects for three types of data: noisy data, incomplete data, and noisy and incomplete data. We fix all the hyper-parameters to the ones used in the main experiment unless otherwise specified. In particular, we set the noise standard deviation to 0.1 for noisy data and the missing rate to 0.5 for incomplete data.

For comparison, we also plot the regrets for the full covariance Gaussian prior baseline. The means and the covariance of the prior are fitted with the three types of imperfect data that are used to train and calibrate the diffusion models, following the procedure detailed in Appendix B.4.

Training from Noisy Data. To cope with noisy data, we add SURE-based regularization with weight λ to our training objective (7). In this part, we focus on how the choice of λ affects the regret when the data are noisy. For the sake of simplicity, we only complete the warm-up phase of the algorithm, that is, the models are only trained for 15000 steps with loss function L and x_ℓ sampled from $X_\ell \,|\, X_0 = y_0$. In our experiments we note this is generally good enough for noisy data without missing entries.

The results are shown in Figure 9. As we can see, the value of λ has a great influence on the regret achieved with the learned prior. However, finding the most appropriate λ for each problem is a challenging task. Using a larger value of λ helps greatly for the `Labeled Arms` problem when it is given the ground-truth standard deviation $\sigma = 0.1$, but is otherwise harmful for the `Popular and Niche` problem. We believe that finding a way to determine the adequate value of λ will be an important step to make our method more practically relevant.

Training from Incomplete Data. The EM step is mainly designed to tackle missing data. In Figure 10 we show how the induced regrets differ when the models are trained with and without it and when the observations are missing at random but not noisy. To make a fair comparison, we also train the model for a total of 24000 (instead of 15000) steps when EM is not employed. As we can see, in all the setups the use of EM results in lower regret.

Training from Incomplete and Noisy Data. To conclude this section we investigate the effects of EM and SURE-based regularization when the data are both noisy and incomplete, as in our main experiment. We either drop totally the regularization term, i.e., set $\lambda = 0$, or skip the EM step (but again we train the models for 24000 steps with the configuration of the warm-up phase in this case). We plot the resulting regrets in Figure 11. For the models without EM, the variance calibration algorithm proposed in Section 4.2 (Algorithm 6) does not work well so we calibrate it with a perfect calibration set $\mathcal{D}_{\text{cal}}$.[13] However, even with this the absence of EM consistently leads to the worst performance. On the other hand, dropping the regularization term only causes clear performance degradation for the `Labeled Arms` problem. This is in line with our results in Figure 9.

D Additional Experiments

In this appendix, we first supplement our numerical section Section 5 with results obtained under different assumed noise levels. After that, we present additional experiments for the posterior sampling and the

[13] Indeed, by design Algorithm 6 only gives good result when the posterior sampling step provides a reasonable approximation of x_0. How to calibrate the variance of a poorly performed model from imperfect data is yet another difficult question to be addressed.

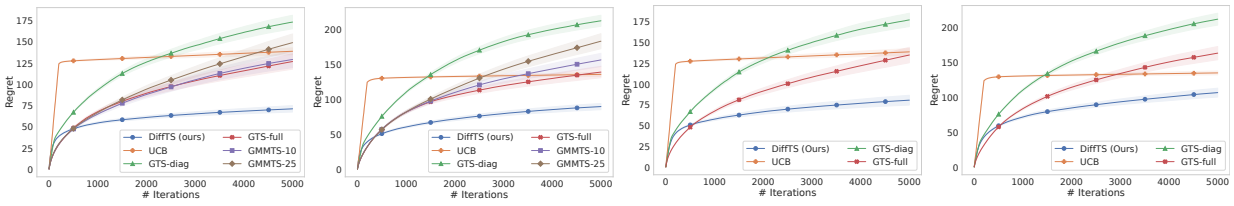

Perfect data $\hat{\sigma} = 0.05$ | Perfect data $\hat{\sigma} = 0.1$ | Imperfect data $\hat{\sigma} = 0.05$ | Imperfect data $\hat{\sigma} = 0.1$

(a) `Popular and Niche`

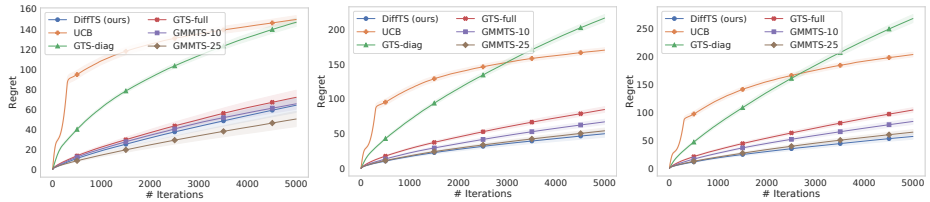

Perfect data $\hat{\sigma} = 0.1$ | Perfect data $\hat{\sigma} = 0.2$ | Perfect data $\hat{\sigma} = 0.3$

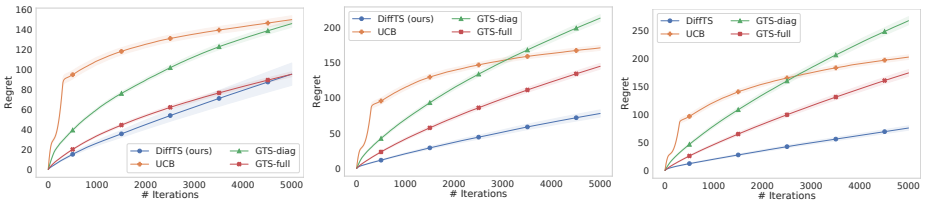

Imperfect data $\hat{\sigma} = 0.1$ | Imperfect data $\hat{\sigma} = 0.2$ | Imerfect data $\hat{\sigma} = 0.3$

(b) `iPinYou Bidding`

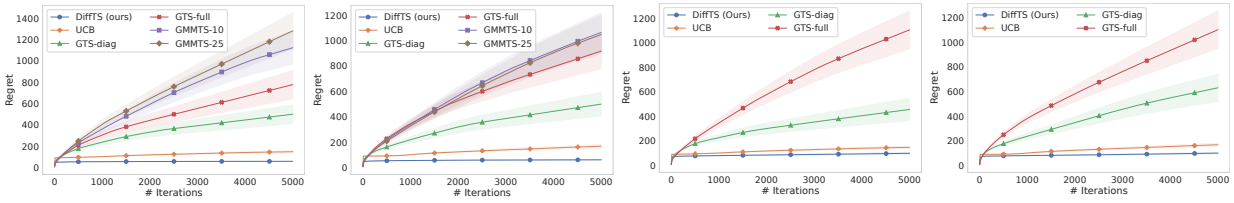

Perfect data $\hat{\sigma} = 0.05$ | Perfect data $\hat{\sigma} = 0.1$ | Imperfect data $\hat{\sigma} = 0.05$ | Imperfect data $\hat{\sigma} = 0.1$

(c) `2D Maze`

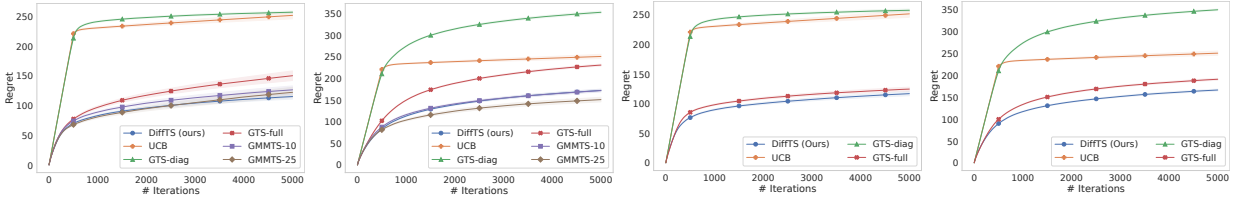

Perfect data $\hat{\sigma} = 0.05$ | Perfect data $\hat{\sigma} = 0.1$ | Imperfect data $\hat{\sigma} = 0.05$ | Imperfect data $\hat{\sigma} = 0.1$

(d) `Labeled Arms`

Figure 12: Regret performances on four different problems with priors fitted/trained on either exact expected rewards (perfect data) or partially observed noisy rewards (imperfect data) and with different assumed noise levels $\hat{\sigma}$. The results are averaged over tasks of a test set and shaded areas represent standard errors.

training algorithms.

D.1 Experimental Results with Different Assumed Noise Levels

To further validate the benefit of diffusion priors, we conduct experiments for the four problems introduced in Appendix B.1 under different assumed noise levels. The results are shown in Figure 12. We see that DiffTS achieves the smallest regret in 15 out of the 18 plots, confirming again the advantage of using diffusion priors. Moreover, although DiffTS performs worse than either GMMTS or GTS-full in `iPinYou Bidding` and `Labled Arms` for a certain assumed noise level, the smallest regret is still achieved by DiffTS when taking all the noise levels that we have experimented with into account.

Finally, it is clear from Figure 12 that the choice of the assumed noise level $\hat{\sigma}$ also has a great influence on the induced regret. The problem of choosing an appropriate $\hat{\sigma}$ is however beyond the scope of our work.

D.2 Comparison of Posterior Sampling Strategies on a Toy Problem

In this part, we demonstrate on a toy problem that using predicted noise $\bar{z}_{\ell+1}$ to construct the diffused observation $\tilde{y}_\ell$ leads to more consistent examples compared to using independently sampled noise vectors.

Data Set and Diffusion Model Training. We consider a simple data distribution over $\mathbb{R}^{200}$. The 200 features are grouped into 20 groups. For each sample, we randomly select up to 6 groups and set the values of the corresponding features to 1. The remaining features take the value 0. Some samples from this distribution are illustrated in Figure 13a. As for the diffusion model, the model architecture, hyper-parameters, and training procedure are taken to be the same as those for the `Popular and Niche` problem (Appendix B). In Figure 13b we see that the data distribution is perfectly learned.

Posterior Sampling. We proceed to investigate the performance of our posterior sampling algorithm on this example. For this, we form a test set of 100 samples drawn from the same distribution and drop each single feature with probability 0.5 as shown in Figure 13c. We then conduct posterior sampling with the learned model using Algorithm 3. To define the diffused observation $\tilde{y}_\ell$, we either follow (4) or replace the predicted noise $\bar{z}_{\ell+1}$ by the sampled noise $\tilde{z}_{\ell+1}$ in the formula. The corresponding results are shown in Figures 13d and 13e. As we can see, using predicted noise clearly leads to samples that are more consistent with both the observations and the learned prior.

To provide a quantitative measure, in the constructed samples we define a group to be 'relevant' if the values of all its features are greater than 0.8. We then compute the recall and precision by comparing the ground-truth selected groups and the ones identified as relevant. When predicted noise is used, the average recall and precision are both at 100%. On the other hand, when independently sampled noise is used, the average recall falls to around 85% (this value varies due to the randomness of the sampling procedure but never exceeds 90%) while the average precision remains at around 98%.

D.3 Training from Imperfect Image Data

To illustrate the potential of the training procedure introduced in Section 4.1, we further conduct experiments on the MNIST and Fashion-MNIST [Xiao et al., 2017] data sets. Both data sets are composed of gray-scale images of size 28×28. MNIST contains hand-written digits whereas Fashion-MNIST contain fashion items taken from Zalando shopping catalog. Some images of the two data sets are shown in Figures 14a and 15a.

Data Corruption and Experimental Setup. For our experiments, we scale the images to range $[0, 1]$ and corrupt the resulting data with missing rate 0.5 (i.e., each pixel is dropped with 50%) and noise of standard deviation 0.1. As we only use training images, this results in 60000 corrupted images for each of the two data sets. We further separate 1000 images from the 60000 to form the calibration sets. We then

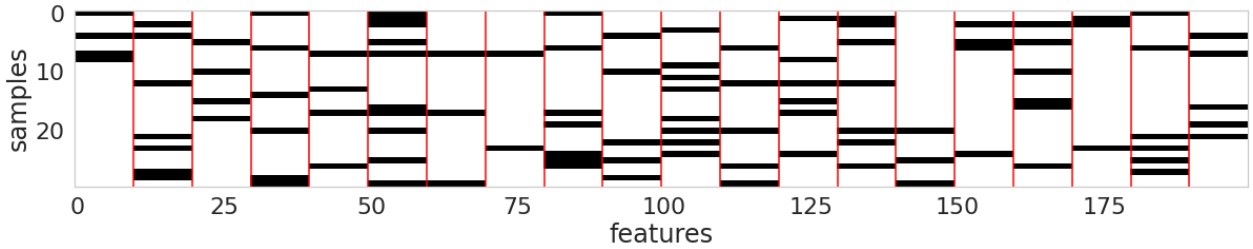

(a) 30 samples from the training set.

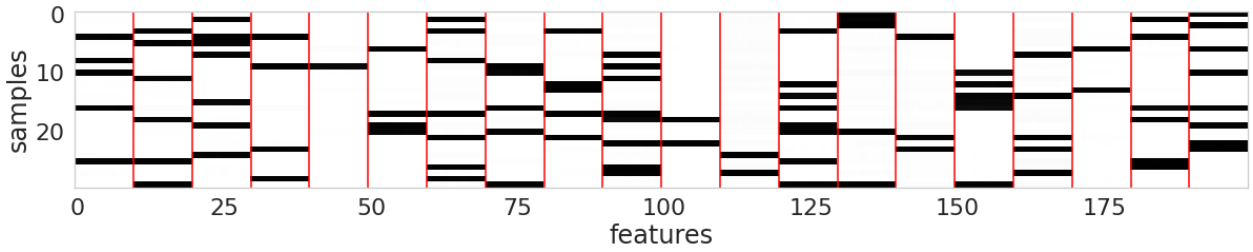

(b) 30 feature vectors generated by the learned diffusion model.

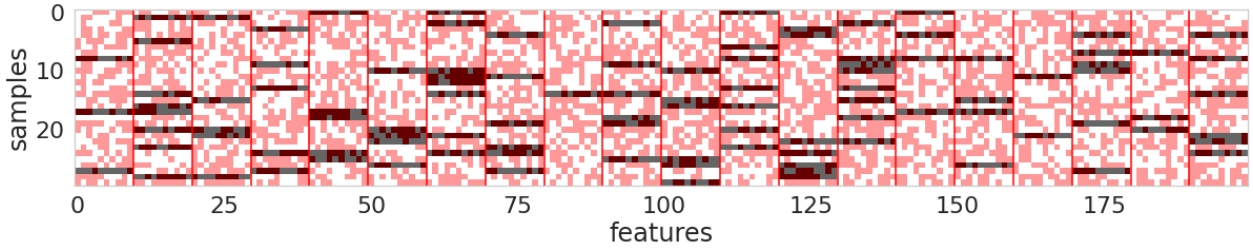

(c) 30 samples from the test set. Red squares indicate missing values.

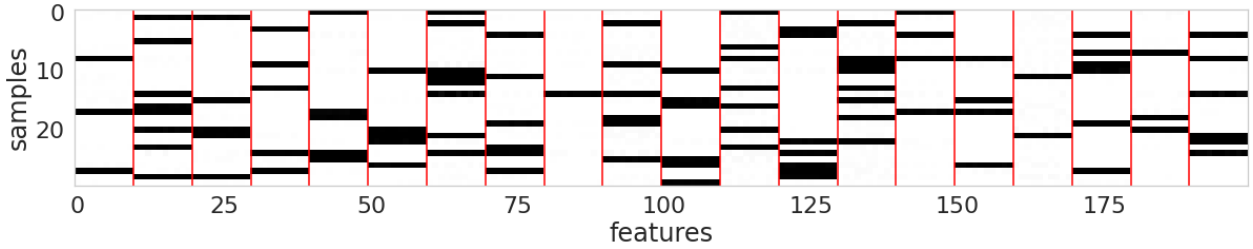

(d) Feature vectors reconstructed with learned diffusion model and Algorithm 3 using predicted noise vectors $\bar{z}_\ell$. The inputs are the ones shown in 13c.

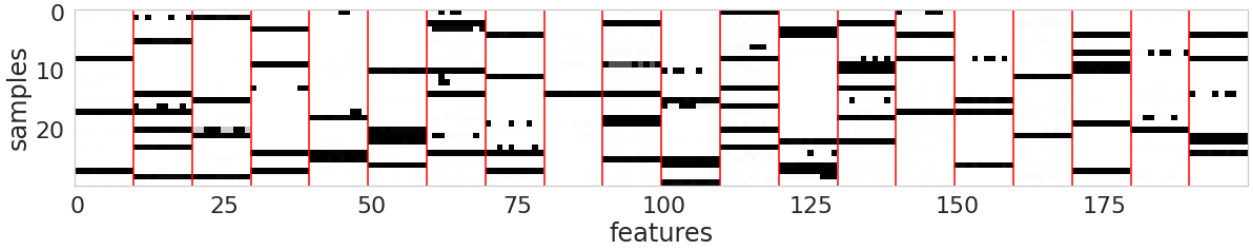

(e) Feature vectors reconstructed with learned diffusion model and Algorithm 3 using independently sampled noise vectors $\tilde{z}_\ell$. The inputs are the ones shown in 13c.

Figure 13: Feature vectors of the toy problems presented in Appendix D.2. Rows and columns correspond respectively to features and samples. For visualization purpose, the features are ordered in a way that those of the same group are put together. The darker the color the higher the value, with white and black representing respectively 0 and 1.

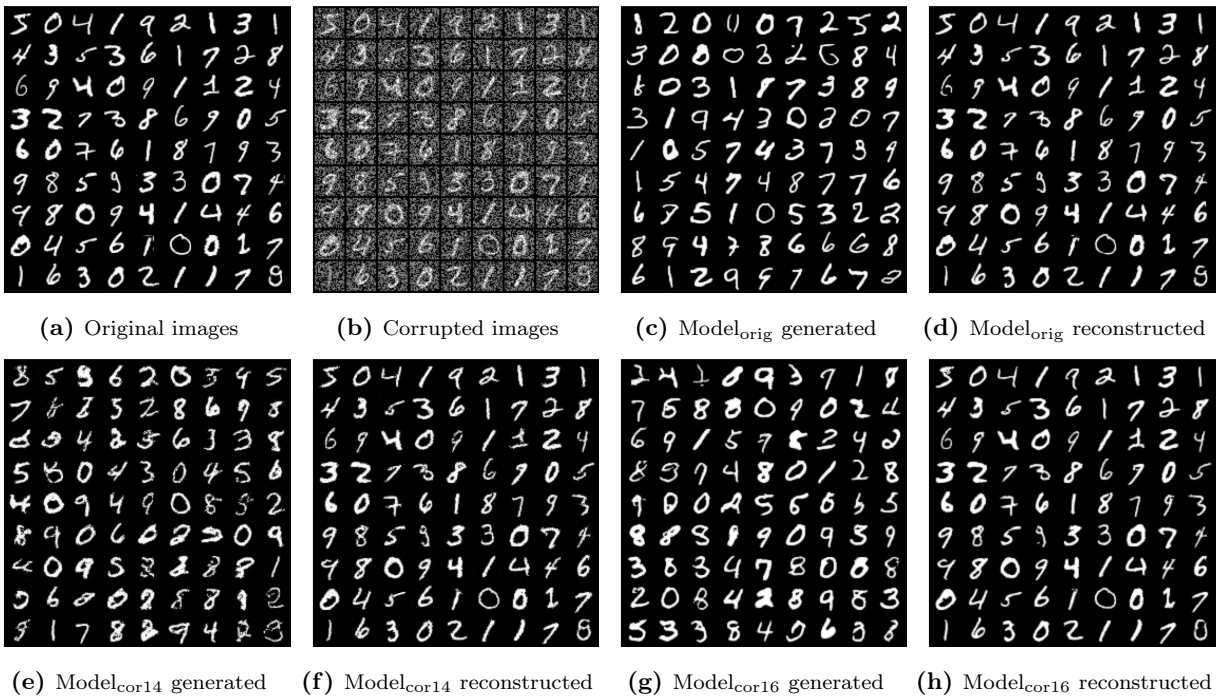

(a) Original images **(b)** Corrupted images **(c)** $\text{Model}_{\text{orig}}$ generated **(d)** $\text{Model}_{\text{orig}}$ reconstructed

(e) $\text{Model}_{\text{cor14}}$ generated **(f)** $\text{Model}_{\text{cor14}}$ reconstructed **(g)** $\text{Model}_{\text{cor16}}$ generated **(h)** $\text{Model}_{\text{cor16}}$ reconstructed

Figure 14: Various images related to the MNIST data set. The three models $\text{Model}_{\text{orig}}$, $\text{Model}_{\text{cor14}}$, and $\text{Model}_{\text{cor16}}$ are respectively trained on the original data set, on the corrupted data set for 14000 steps, and on the corrupted data set for 16000 steps ($\text{Model}_{\text{cor16}}$ is trained on top of $\text{Model}_{\text{cor14}}$ for another 2000 steps; see the text for more details). 'Generated' means unconditional sampling while 'reconstructed' means posterior sampling with Algorithm 3 applied to the corrupted images shown in (b).

train the diffusion models from these corrupted images following Algorithm 5, with $S = 5000$ warm-up steps, $J = 3$ repeats of the EM procedure, and $S' = 3000$ inner steps for each repeat (the total number of training steps is thus 14000). The learning rate and the batch size are respectively fixed at 10^{-4} and 128.

For the regularization term, we take $\lambda = 0.2$ for MNIST and $\lambda = 0.1$ for Fashion-MNIST. The constant ε is set to 10^{-5} as before. As in Ho et al. [2020], Song et al. [2020], we note that the use of exponential moving average (EMA) can lead to better performance. Therefore, we use the EMA model for the posterior sampling step. The EMA rate is 0.995 with an update every 10 training steps. For comparison, we also train diffusion models on the original data sets with the aforementioned learning rate and batch size for 10000 steps. Finally, to examine the influence of the regularization weight λ on the generated images, we consider a third model for MNIST trained on top of the 14000-step model with corrupted data. For this model, we perform an additional posterior sampling step and then train for another 2000 steps with $\lambda = 1$. The remaining details, including the model architecture, are the same as those for the `2D Maze` experiment.

Results. In Figures 14 and 15, we show images from the original data set, from the corrupted data set, and produced by the trained models either by unconditional sampling or data reconstruction with Algorithm 3. Overall, our models manage to generate images that resemble the ones from the original data set without overly sacrificing the diversity.

Nonetheless, looking at the samples for Fashion-MNIST we clearly see that a lot of details are lost in the images generated by or reconstructed with diffusion models. In the case of training from perfect data, this can clearly be improved with various modifications to the model including change in model architecture, number of diffusion steps, and/or sampling algorithms [Karras et al., 2022]. This would become more challenging in the case of training from imperfect data as the image details can be heavily deteriorated by noise or missing pixels.

On the other hand, the effect of the regularization parameter λ can be clearly seen in the MNIST

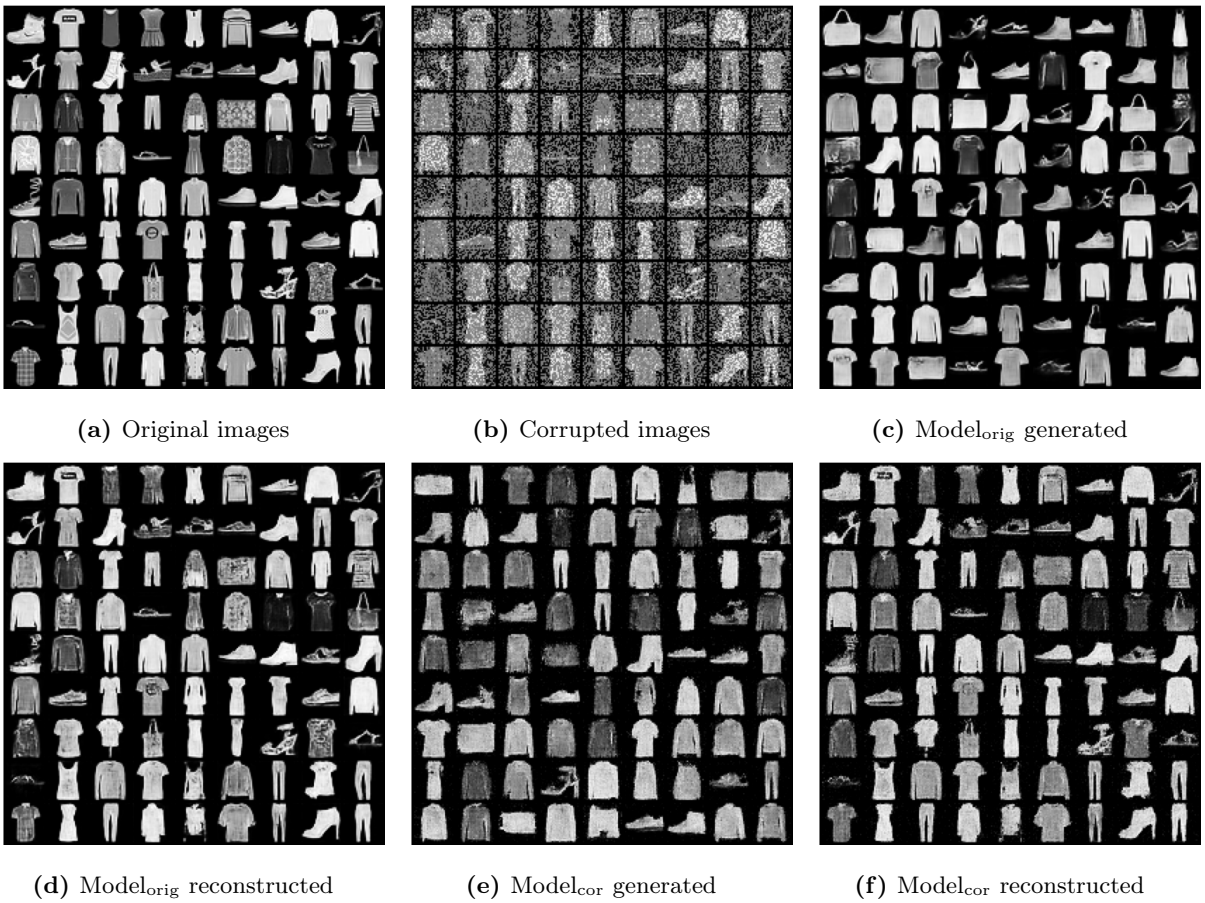

(a) Original images **(b)** Corrupted images **(c)** $\text{Model}_{\text{orig}}$ generated

(d) $\text{Model}_{\text{orig}}$ reconstructed **(e)** $\text{Model}_{\text{cor}}$ generated **(f)** $\text{Model}_{\text{cor}}$ reconstructed

Figure 15: Various images related to the Fashion-MNIST data set. The two models $\text{Model}_{\text{orig}}$ and $\text{Model}_{\text{cor}}$ are respectively trained on the original data set and the corrupted data set. 'Generated' means unconditional sampling while 'reconstructed' means posterior sampling with Algorithm 3 applied to the corrupted images shown in (b).

experiment from Figure 14. Larger λ enables the model to produce digits that are more 'connected' but could cause other artifacts. As in any data generation task, the definition of a good model, and accordingly the appropriate choice of λ, varies according to the context.

To summarize, we believe that the proposed training procedure has a great potential to be applied in various areas, including training from noisy and/or incomplete image data, as demonstrated in Figures 14 and 15. However, there is still some way to go in making the algorithm being capable of producing high-equality samples for complex data distribution.

E Expected Reward Visualization

In Figures 16 to 21 we provide various visualizations of the bandit mean reward vectors either of the training sets or generated by the learned priors.

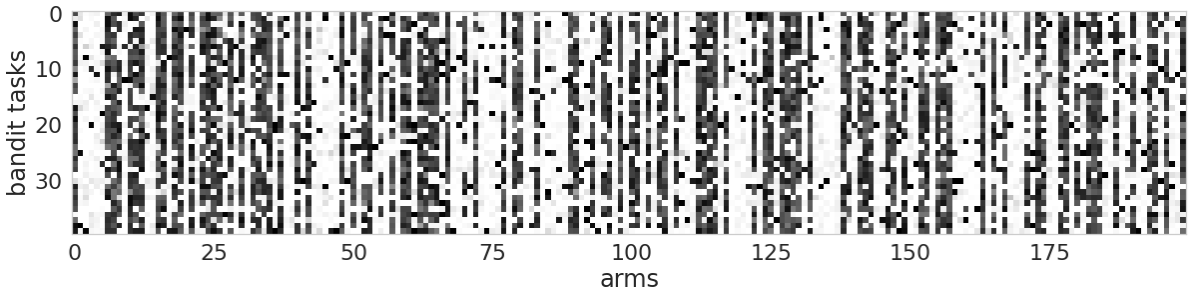

(a) 40 samples from the perfect training set $\mathcal{D}_{\text{tr}}$.

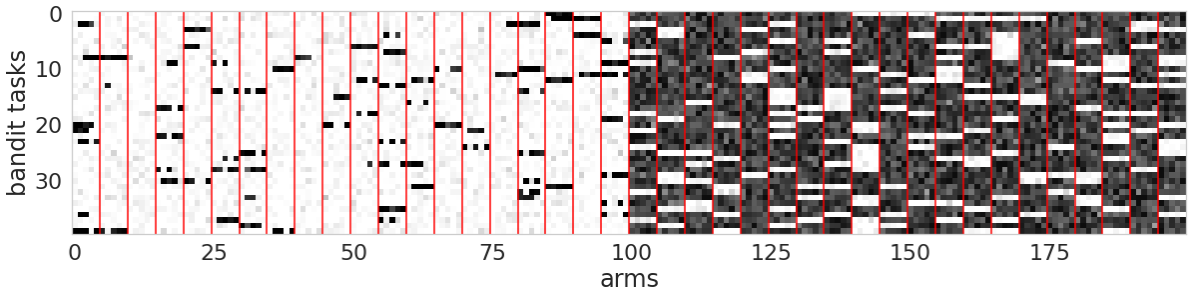

(b) 40 samples from the perfect training set $\mathcal{D}_{\text{tr}}$, reordered to put the arms of the same group together. The popular arms are on the right side of the figure.

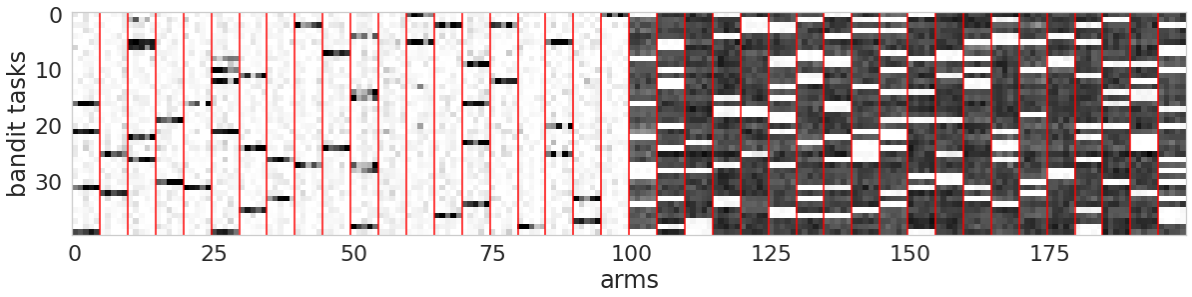

(c) 40 mean reward vectors generated the diffusion model trained on perfect data, reordered to put the arms of the same group together. The popular arms are on the right side of the figure.

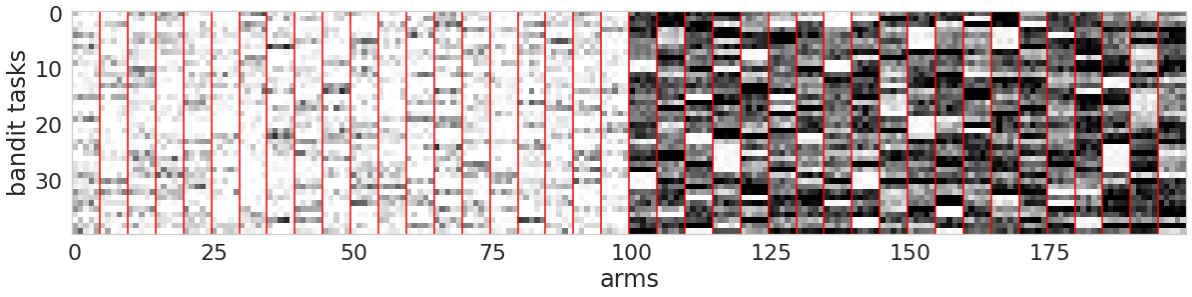

(d) 50 mean reward vectors generated by the 25-component GMM fitted on perfect data, reordered to put the arms of the same group together. The popular arms are on the right side of the figure.

Figure 16: Visualization of the mean reward vectors of the `Popular and Niche` problem. Rows and columns correspond to tasks and arms. The darker the color the higher the value, with white and black representing respectively 0 and 1. Diffusion models manage to learn the underlying patterns that become recognizable by humans only when the arms are grouped in a specific way.

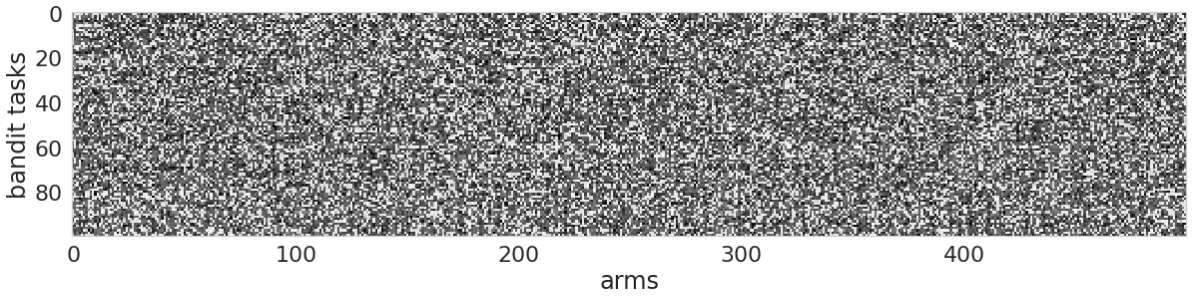

(a) 100 samples from the perfect training set $\mathcal{D}_{\text{tr}}$.

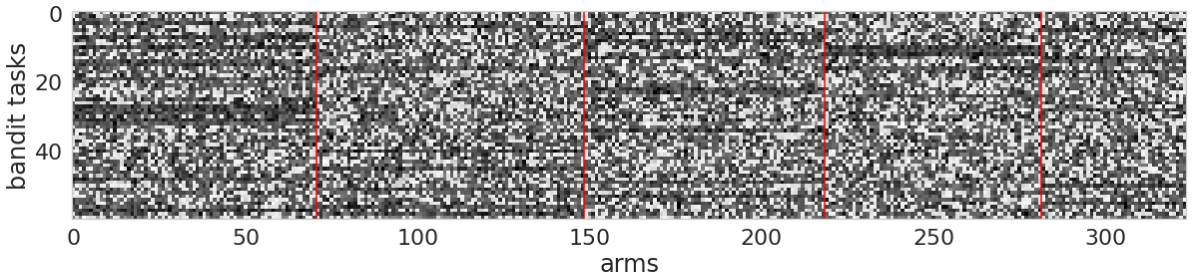

(b) 60 samples from the perfect training set $\mathcal{D}_{\text{tr}}$, grouped by labels and showing only 5 labels. Note that each arm has multiple labels and thus appears in multiple groups.

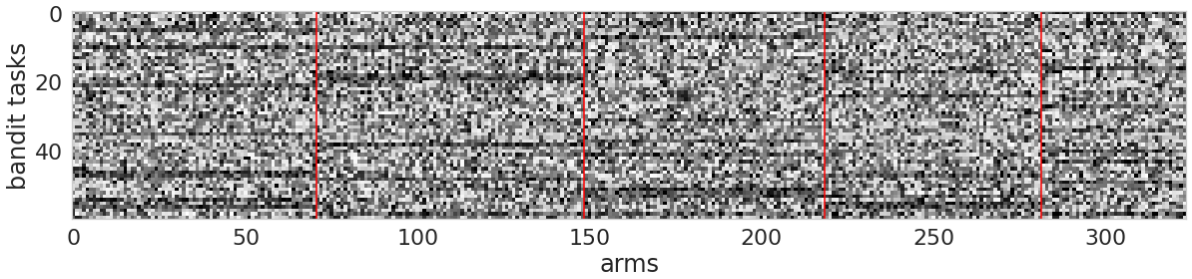

(c) 60 mean reward vectors generated by the diffusion model trained on perfect data, grouped by labels and showing only 5 labels. Note that each arm has multiple labels and thus appears in multiple groups.

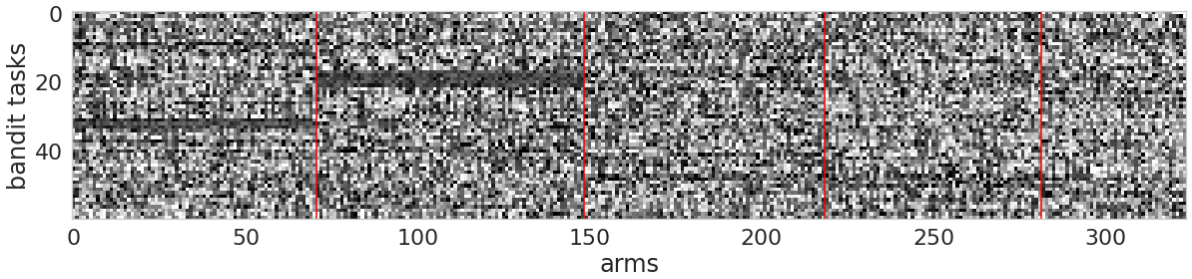

(d) 60 mean reward vectors generated by the 25-component GMM fitted on perfect data, grouped by labels and showing only 5 labels. Note that each arm has multiple labels and thus appears in multiple groups.

Figure 17: Visualization of the mean reward vectors of the `Labeled Arms` problem. Rows and columns correspond to tasks and arms. The darker the color the higher the value, with white and black representing respectively 0 and 1. While human eyes can barely recognize any pattern in the constructed vectors, diffusion models manage to learn the underlying patterns that become recognizable by humans only when the arms are grouped in a specific way.

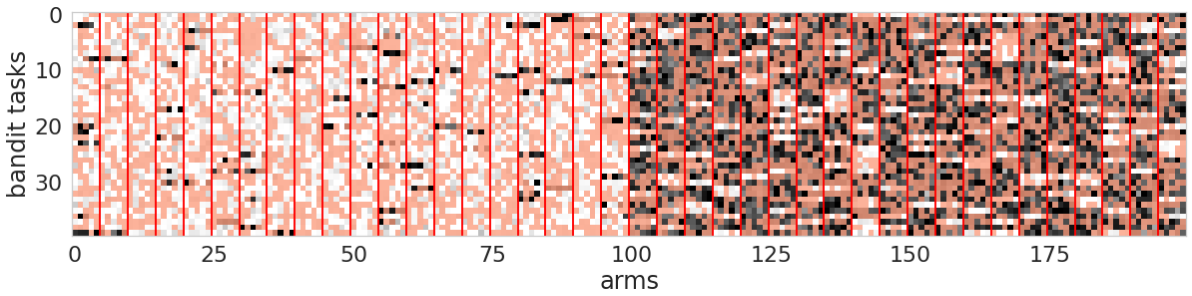

(a) 40 samples from the imperfect training set $\check{\mathcal{D}}_{\text{tr}}$. Red squares indicate missing values.

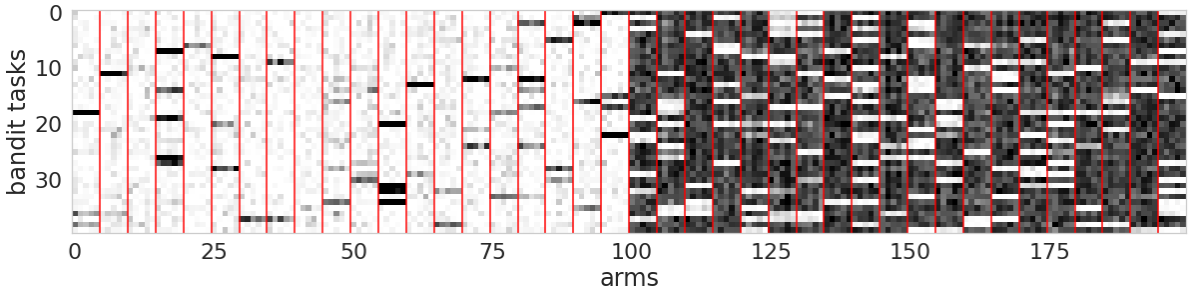

(b) 40 mean reward vectors generated by the diffusion model trained on imperfect data.

Figure 18: Mean reward vectors of the `Popular and Niche` problem. Rows and columns correspond to tasks and arms. For ease of visualization, the arms are reordered so that arms of the same group are put together and popular arms are on the right of the figures. The darker the color the higher the value, with white and black representing respectively 0 and 1.

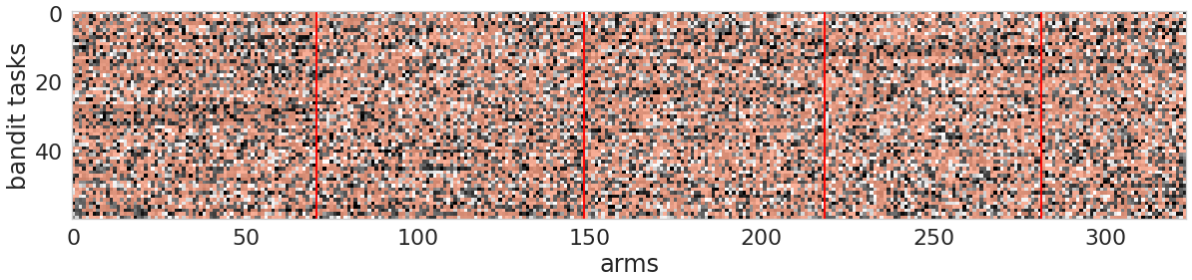

(a) 60 samples from the imperfect training set $\check{\mathcal{D}}_{\text{tr}}$. Red squares indicate missing values.

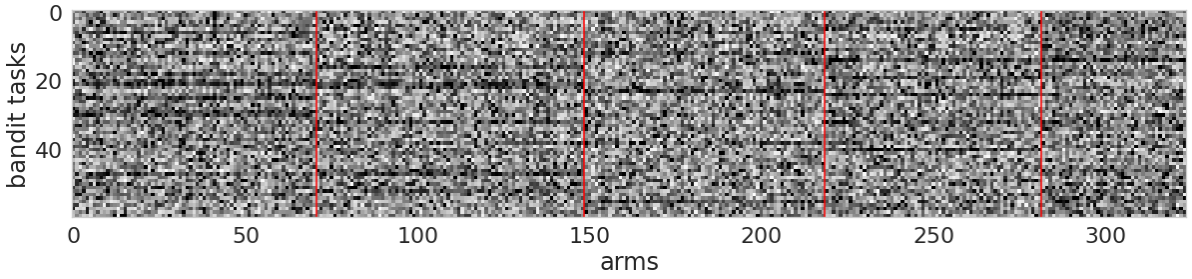

(b) 60 mean reward vectors generated by the diffusion model trained on imperfect data.

Figure 19: Mean reward vectors of the `Labeled Arms` problem. Rows and columns correspond to tasks and arms. For ease of visualization, the arms are grouped by labels and only arms that are associated to 5 labels are shown. The darker the color the higher the value, with white and black representing respectively 0 and 1.

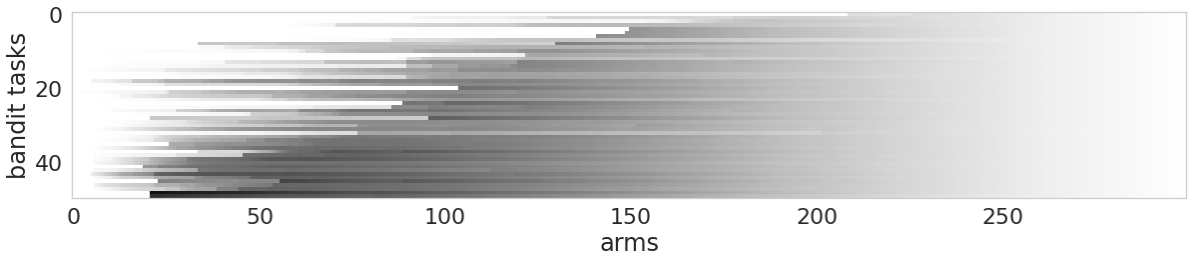

(a) 50 samples from the perfect training set $\mathcal{D}_{\text{tr}}$.

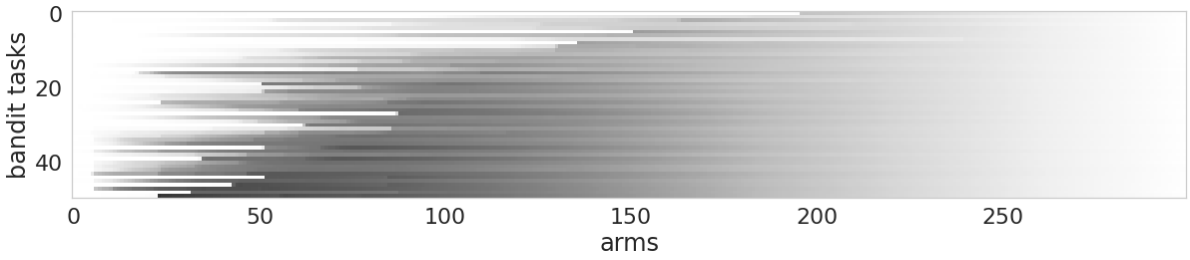

(b) 50 mean reward vectors generated by the diffusion model trained on perfect data.

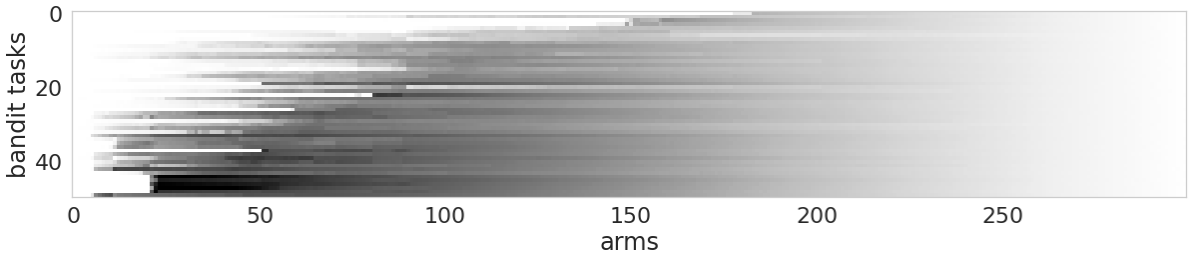

(c) 50 mean reward vectors generated by the 25-component GMM fitted on perfect data.

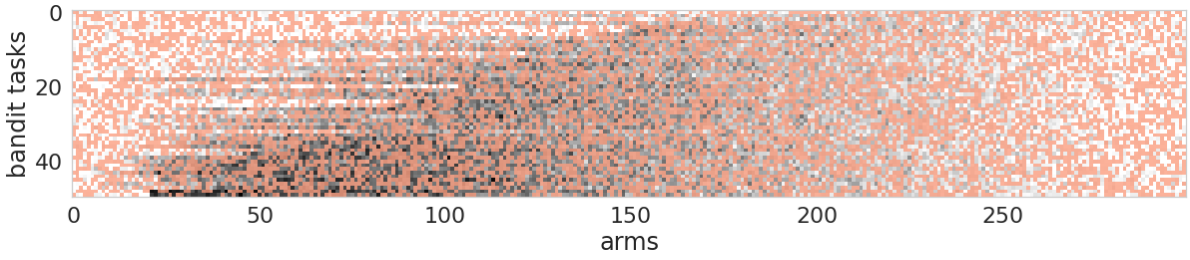

(d) 50 samples from the imperfect training set $\check{\mathcal{D}}_{\text{tr}}$. Red squares indicate missing values.

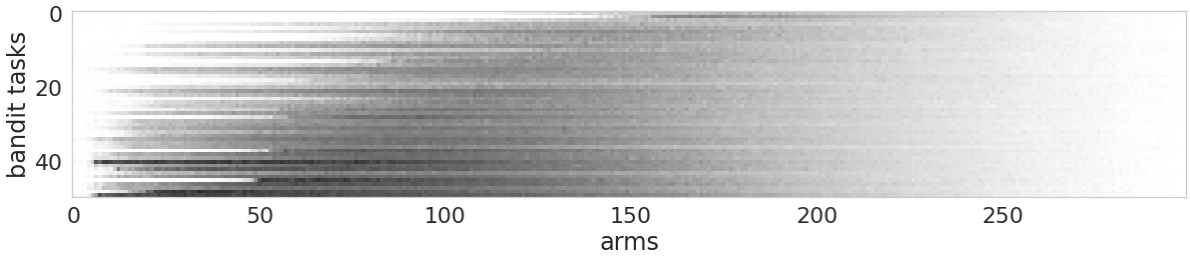

(e) 50 mean reward vectors generated by the diffusion model trained on imperfect data.

Figure 20: Mean reward vectors of the `iPinYou Bidding` problem. Rows and columns correspond respectively to tasks and arms. For visualization purpose, we order the tasks by the position of their optimal arm. The darker the color the higher the value, with white and black representing respectively 0 and 1.

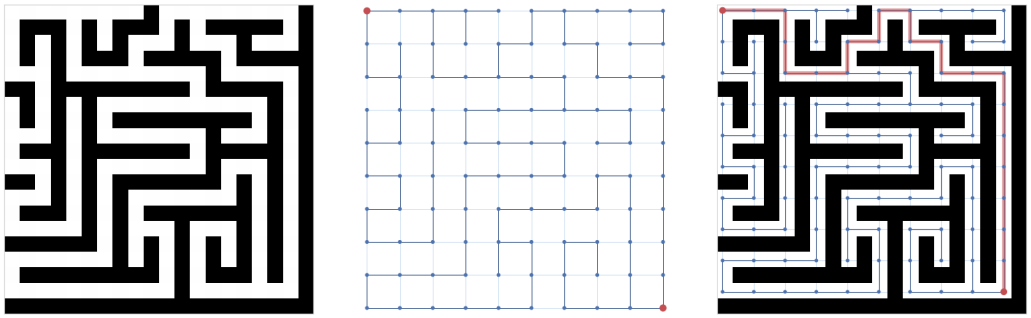

(a) Sample from the perfect training set $\mathcal{D}_{\text{tr}}$.

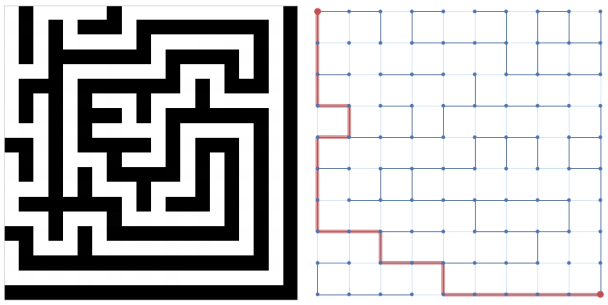

(b) Sample generated by the diffusion model trained on perfect data.

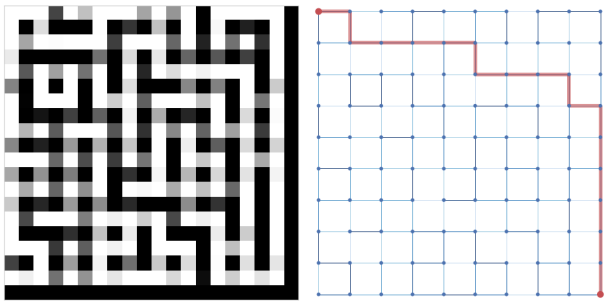

(c) Sample generated by the 25-component GMM fitted on prefect data.

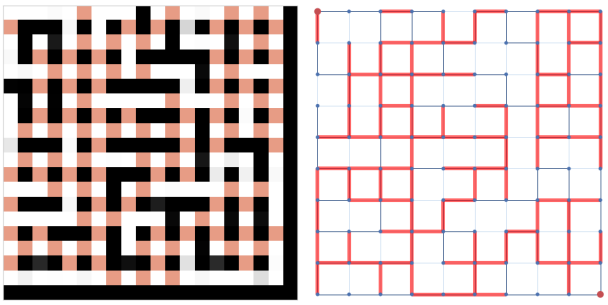

(d) Sample from the imperfect training set $\check{\mathcal{D}}_{\text{tr}}$. Red squares and edges indicate missing values.

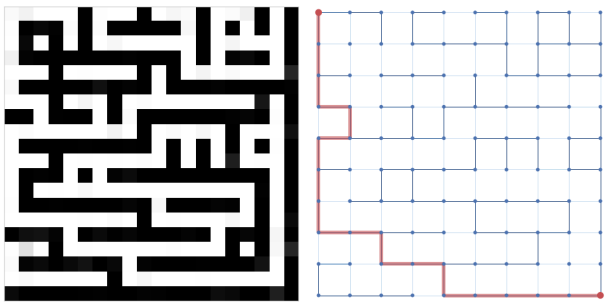

(e) Sample generated by the diffusion model trained on imperfect data.

Figure 21: The weighted grid graphs and the corresponding 2D maze representations of the `2D Maze` problem. For visualization, the weights (mean rewards) are first clipped to $[-1, 0]$. Then, for the grid graphs darker the color higher the mean reward (i.e., closer to 0) while for the maze representations it is the opposite. Also note that for the maze representations only a part of the pixels correspond the the edges of the grid graphs, while the remaining pixels are filled with default colors (black or white). The red paths indicate the optimal (super-)arms.